LUND UNIVERSITY

# Modelling and Experimental Investigations on Thermal Radiation in Combustion Environments

Hofgren, Henrik

2015

# Modelling and Experimental Investigations on Thermal Radiation in Combustion Environments

Henrik Hofgren


LUND
UNIVERSITY

Thesis for the degree of Doctor of Philosophy in Engineering, 2015

Division of Heat Transfer
Department of Energy Sciences
Faculty of Engineering (LTH)
Lund University
www.energy.lth.se

Division of Heat Transfer
Department of Energy Sciences
Faculty of Engineering (LTH)
Lund University
P.O. Box 118, SE-221 00, Lund, Sweden

ISBN 978-91-7623-353-5
ISRN LUTMDN/TMHP-15/1111-SE
ISSN 0282-1990

# Abstract

Thermal radiation is an important physical phenomenon in combustion environments. For the understanding of existing- and the design of new combustion environments computational modelling is a useful tool as it can describe the different transport phenomena. This thesis has focused on studying thermal radiative property models of the participating media, gases and particles. Two specific combustion environments have also been studied, from a thermal radiation perspective. The focus is on radiative property models that are useful specifically for engineering purposes. These property models are often developed from more advanced spectral models by means of correlative or other methods to simplify the treatment of the radiative transfer. One such model is the non-correlated statistical narrow band (SNB) model, which drops spectral relation between intensity and transmissivity, which is used in the correlated SNB model. By doing so a significant decrease in computational demand can be achieved. The accuracy of this model has been questioned in the literature although it has been suggested as an appropriate option for sooty environments. The assessment of the model revealed that it only gives good predictions in large geometries and highly sooty environments. Because of the model's limited applicability and a still rather high computational demand it is not recommended for use even in sooty environments. A simpler model, and computationally much faster, called the weighted sum of gray gas (WSGG) model accompanied the assessment of the non-correlated SNB model. The WSGG model was shown to be a better choice than the non-correlated SNB model in sooty environments. A gray gas property model was compared with a WSGG model in combustion environments resembling the ones found in grate fired furnaces. In these environments, which also contains particles, the gray model was shown to give predictions of wall heat flux in close agreement with the WSGG model. This shows how the simplest model, which the gray model is, can sometimes be a suitable choice, especially when particles are present. Particle property models were evaluated in various combustion environments. A common approach is to use Planck mean coefficients to represent the particle properties. The use of Planck mean coefficients for fly-ash particles, common in furnaces combusting solid fuels, is shown to give large errors in prediction of both radiative heat flux and the source term in particular.

The two investigated combustion environments are those found in grate fired furnaces and environments with high CO mole fraction. The grate fired furnace was studied in both modelling- and measurement work. Specifically the importance of particle radiation was investigated in the grate fired combustion environment. A preliminary study of the grate fired furnace was a parametric study. The parameters investigated were different particles originating from combustion of biomass and municipal solid waste, different furnace size, and boundary emissivities. The most significant effect on the overall radiative heat transfer is that of particles from municipal solid waste; moderate effects are seen when particles come from biomass. Increased furnace size most affected the heat flux to the hot bed and source term compared with a case without any particles. The choice of emissivity can be as important as considering particles or not. The measurement and modelling work were carried out on a 400 kW grate fired furnace combusting biomass. The boundary temperatures, flue gas temperature, gas mole fraction, particle mass-size distribution, and wall irradiation were measured. A so-called indirect wall irradiation was retrieved when the furnace was modelled with the implemented measured parameters. This indirect wall irradiation was compared with the directly measured wall irradiation. The study revealed that particle radiation is very important in the evaluated furnace, it doubles the wall irradiation in the hot flame zone compared with irradiation only from gases. The CO contribution to the total directional radiation was studied in environments with high mole fractions of CO, often found in gasifiers. CO is normally disregarded in environments where the fuel is fully oxidised, as it is a weak radiating species and small mole fractions of CO exist in these types of environments. The evaluation reveal that disregarding CO is still a good approach even in gasifier environments. These environments still contain small volume fractions of $CO_2$ and $H_2O$, which compared with CO are much stronger radiators. The rotational-vibrational bands of these two species overlaps the important fundamental band of CO reducing the importance of CO to the total directional radiative heat flux.

# Populärvetenskaplig sammanfattning

Värmestrålning är högst relevant i förbränningsmiljöer. I dessa miljöer är förbränningsgaser och partiklar den huvudsakliga källan till värmestrålning. Förbränningsmiljön är komplex att beskriva. Analys av turbulenta flöden, kemiska reaktioner och transport av energi måste göras för att fullständigt beskriva miljön. Att kunna beskriva dessa fenomen är en viktig del i förståelsen av miljön men även för att kunna designa nya förbränningsmiljöer. Värmestrålning är en del av den energitransport som sker i förbränningsmiljön. Denna avhandling behandlar specifikt ett urval av de modeller som beskriver hur gaser och partiklar avger och tar upp värmestrålning, så kallade egenskapsmodeller. Två specifika förbränningsmiljöer har även studerats med avseende på värmestrålning, förbränningsmiljöer med hög andel kolmonoxid och de som existerar i rosterpannor.

Vatten i gasform och koldioxid är de gaser som huvudsakligen inverkar på värmestrålningen men även andra gaser kan bidra, t ex metan och kolmonoxid. Sot är en partikel som förekommer i många förbränningsmiljöer. I de miljöer som eldar fasta bränslen, t ex biomassa, kol eller avfall, kan bränslepartiklar och aska även finnas. Resultaten från studier av egenskapsmodeller visar att då en viss andel partiklar finns i förbränningsmiljön så är det inte alltid motiverat att använda alltför avancerade egenskapsmodeller för gaserna. Enkla modeller kan prediktera likvärdiga resultat för värmestrålningen med avsevärt mindre behov av dataresurser. Detta beror på att partiklar börjar dominera upptagandet och avgivandet av värmestrålning jämfört med gaserna. Olika egenskapsmodeller för partiklar kan även påverka hur väl värmestrålningen predikteras. Väldigt ofta används enkla egenskapsmodeller för partiklar. För aska, kan dessa enkla egenskapsmodeller kan ge stora fel i uppskattningen av värmestrålningen. Resultaten från studier av egenskapsmodeller i denna avhandling guidar oss till några av de modeller som kan användas och vilka som skall undvikas.

Kolmonoxid är en gas som har en mindre växelverkan med strålning än de två vanligaste gaserna, vatten och koldioxid. Av denna anledning så försummas oftast värmestrålningen från kolmonoxid. I förgasningsmiljöer kan volymandelen av kolmonoxid vara upp mot och över 50%. Detta är en väldigt hög andel jämfört med vanliga förbränningsmiljöer. Av denna anledning är det intressant att undersöka om kolmonoxid fortfarande går att bortse ifrån i

förgasningsmiljöer, då värmestrålningen till väggarna avses. Denna avhandling visar att bidraget från kolmonoxiden fortfarande kan försummas i förgasningsmiljöer. Detta beror på att det oftast också finns små mängder av koldioxid och vatten vilka, på grund av dess starka strålningsegenskaper, överskuggar bidraget från kolmonoxiden. Den andra förbränningsmiljön som studerades var rosterpannan. Rosterpannan är en förbränningsteknologi som förbränner fasta bränslen. Förbränningen av bränslet startar längst ner i pannan på rostern och försätter ovan i förbränningsrummet av de brännbara gaser och partiklar som lämnar bränslebädden. I denna avhandling har fokus varit på värmestrålningen i förbränningsrummet. Både modelleringsstudier och experimentella studier har genomförts på olika rosterpannor. En första utredning av värmestrålning i rosterpannan var en parameterstudie. Parametrarna som studerades var partikelmängder från avfall och biomassa, storlekar på pannan och strålningsegenskaper för pannans ytor. Mest partiklar skapas vid förbränning av avfall så detta bränsle hade störst inverkan på värmestrålningen. Generellt ökade värmestrålningen till väggarna i pannan när storleken ökade. Valet av strålningsegenskaper för väggar och bädd visade sig ha stor inverkan på värmestrålningen. En 400 kW rosterpanna i pilotskala studerades genom att utföra mätningar och modellering. Mätningarna som utfördes på rosterpannan har inte tidigare utförts på någon rosterpanna. Uppmätt data användes som en input till modellering av pannan vilket möjliggjorde en djupare studie av värmestrålningen i pannan. Studien av pilotpannan visade att partiklar kan ha en stor inverkan på värmestrålningen till väggarna. Då partiklar betraktades så fördubblades värmestrålningen till väggarna i pannans nedre delar.

# Acknowledgements

My main supervisor and professor, Bengt Sundén, is kindly acknowledged for his input, work, and support through the years of my doctoral studies. My co-supervisors Thomas Norman and Zhenghua Yan are kindly acknowledged for their contributions. I also want to acknowledge Lei Wang for his input, expertise, and cooperation during the experimental work on the grate fired test furnace. A special thanks needs to be sent to Stefan Svensson at the department of Fire Safety Engineering and Anders Gudmundsson at the department of Ergonomics and Aerosol Technology at Lund University for lending out and giving instructions to important equipment used during the experimental work on the grate fired test furnace.

The financial support of E.ON Sweden AB, the Swedish Energy Agency, and Babcock & Wilcox Vølund A/S is kindly acknowledged

# List of publications

This thesis is based on the following papers. In the body of the text in the thesis the papers will be referred to with roman nummericals, as given below.

I **H. Hofgren**, Z. Yan, B. Sundén, Extension of a fast narrow band model for calculation of thermal radiation in combustion environments with high CO concentration, in 6th International Symposium on Radiative Transfer, Antalya, Turkey, p. 10, 2010

II **H. Hofgren**, B. Sundén, Modelling thermal radiation with the focus on particle radiation in grate fired furnaces combusting MSW or biomass – A parametric study, in ASME 2013 International Mechanical Engineering Congress and Exposition, San Diego, USA, p. 10, 2013

III **H. Hofgren**, B. Sundén, Evaluation of Planck mean coefficients for particle radiative properties in combustion environments, Heat and Mass Transfer, 51(4), pp. 507-519, 2015

IV **H. Hofgren**, B. Sundén, L. Wang, T. Norman, M. Mandø, Measurements of some characteristics of thermal radiation in a 400 kW grate fired furnace combusting biomass, submitted, p. 18, 2015

V **H. Hofgren**, B. Sundén, L. Wang, T. Norman, M. Mandø, Computation of radiative heat transfer in a 400 kW grate fired furnace combusting biomass, in Eurotherm 105, Computational Thermal Radiation in Participating Media V, Albi and Toulouse, France, p. 13, 2015

VI **H. Hofgren,** B. Sundén, Assessment of a non-correlated SNB in sooting environments, submitted, p. 7, 2015

## Author contribution

The thesis author was responsible for writing the papers. In the modelling papers, I-III, V, VI, the author was responsible for setting up models, producing, and evaluating results. Co-authors contributed by revising the papers. For the experimental paper, IV, the co-other authors also contributed in carrying out measurements and error analyses of the measurements.

# Nomenclature

## Latin symbols

| | | |
|---|---|---|
| a | Black body weight | [-] |
| $a_n$, $b_n$ | Mie coefficients | [-] |
| $A_v$ | Avogadro number | [1/mol] |
| c | Black body weighting coefficient | [-] |
| c | Particle distance | [m] |
| C | Correlation coefficient for the black body weighs | [-] |
| $c_0$ | Speed of light in vacuum | [m/s] |
| $C_0$ | Soot constant | [-] |
| $C_2$ | Second Planck constant | [m.K] |
| C | Cross section | [$m^2$] |
| d | Line distance | [m] |
| D | Diameter | [m] |
| E | Emissive power | [$W/m^2$] |
| E´´ | Lower state energy | [J] |
| $f_k$ | Line shape profile | [-] |
| $f_v$ | Soot volume fraction | [-] |
| g | Asymmetry factor | [-] |
| h | Planck constant | [Js] |
| H | Irradiation | $W/m^2$ |
| I | Intensity | [$W/m^2$ sr] |
| $\hat{\imath}$ | Prinicipal direction | [-] |
| $\hat{\jmath}$ | Prinicipal direction | [-] |
| $\hat{k}$ | Prinicipal direction | [-] |
| k | Boltzmann´s constant | [J/K] |
| k | Absorptive index of refraction | [-] |
| K | Correlation coefficient for the gray gas absorption coefficient | [-] |
| m | Mass | [kg] |
| m | Complex index of refraction | [-] |
| n | Refractive index | [-] |
| $\hat{n}$ | Surface normal | [-] |

| | | |
|---|---|---|
| N | Molecular mole density | [mol/dm$^3$] |
| P | Probability distribution | [-] |
| P | Total pressure | [Pa] |
| $p_c$ | Partial pressure | [Pa] |
| q | Heat flux | [W/m$^2$] |
| Q | Internal partition function | [-] |
| Q | Efficiency factor | [-] |
| r | position vector | [m] |
| R | Universal gas constant | [J/K mol] |
| s | Path length | [m] |
| $\hat{s}$ | direction | [-] |
| S | Line strength | [-] |
| $S_1$, $S_2$ | Amplitude functions | [-] |
| T | Temperature | [K] |
| u | Optical depth | [m$^4$ Pa/kg] |
| W | Equivalent line width | [-] |
| w | Quadrature weights | [-] |
| x | position | [m] |
| x | Mole fraction | [-] |
| x | Size parameter | [-] |

## Greek symbols

| | | |
|---|---|---|
| α | Absorbtivity | [m/kg] |
| β | Extinction | [1/m] |
| γ | Line broadaning | [1/m] |
| ε | Emissivity | [-] |
| η | Wavenumber | [1/m] |
| $\eta_0$ | Wavenumber in line center | [1/m] |
| $\eta_i$ | Position of fundamental vibration band | [1/m] |
| θ | Polar angle | [rad] |
| Θ | Scattering angle | [rad] |
| κ | Absorption coefficient | [1/m] |
| λ | Wavelength | [m] |
| μ | Direction cosine | [-] |
| ρ | Density | [kg/m$^3$] |
| ρ | Reflectivity | [-] |
| σ | Stefan Boltzmann´s constant | [W/m$^2$ K$^4$] |
| $\sigma_s$ | Scattering coefficient | [1/m] |
| τ | Transmissivity | [-] |
| φ | Azimuthal angle | [rad] |

| | | |
|---|---|---|
| $\Phi$ | Scattering phase function | [-] |
| $\Omega$ | Solid angle | [sr] |

## Subscript

| | |
|---|---|
| 0 | Reference state |
| abs | Absorption |
| air | Air broadening |
| b | Black body |
| eq | Equivalent parameter |
| ext | Extinction |
| i | Gray gas |
| i | Index direction |
| i | Species |
| i | Spectral position index |
| i | Particle size index |
| j | Index direction |
| j | Polynomial coefficient |
| k | Spatial position |
| k | Line |
| mix | Mixture of species |
| n | Spatial position |
| P | Planck coefficient |
| part | Particle |
| ref | Reference state |
| sca | Scattering |
| self | Self-broadening |
| w | Wall |
| xi | Spatial position |
| $\Delta\eta$ | Narrow band |

## Abbreviations

| | |
|---|---|
| ADF | Absorption distribution function |
| CFD | Computational fluid dynamics |
| DOM | Discrete ordinates method |
| DTM | Discrete transfer method |
| EWBM | Exponential wide band model |
| FSK | Full spectrum correlated-k distribution |
| FVM | Finite volume method |
| HG | Henyey-Greenstein |

| | |
|---|---|
| LBL | Line-by-line |
| MBL | Mean beam length |
| MSW | Municipal solid waste |
| PAH | Polycyclic aromatic hydrocarbon |
| RTE | Radiative transfer equation |
| SLW | Spectral line weighted sum of gray gas |
| SNB | Statistical narrow band |
| WSGG | Weighted sum of gray gas |

# Contents

# 1 Introduction

Research related to combustion spans a wide range of fields such as chemical reactions and kinetics, turbulent flow, material science, thermal radiation, etc. It is an important field of research as most of the world's energy consumption relates to thermochemical conversion, such as combustion, of carbon-based fuels. Close to 87 percent [1] of the world's total energy consumption in 2013 came from carbon-based fuels, not counting biomass, peat, and waste. The use of carbon-based fuels is continuously increasing, as shown in figure 1.1, and it is estimated that coal-based fuel will last 100 to 200 years more depending on world consumption rates [2]. As energy is anticipated to come from carbon-based fuels for quite a long time it is therefore important that it is utilised in an efficient way.

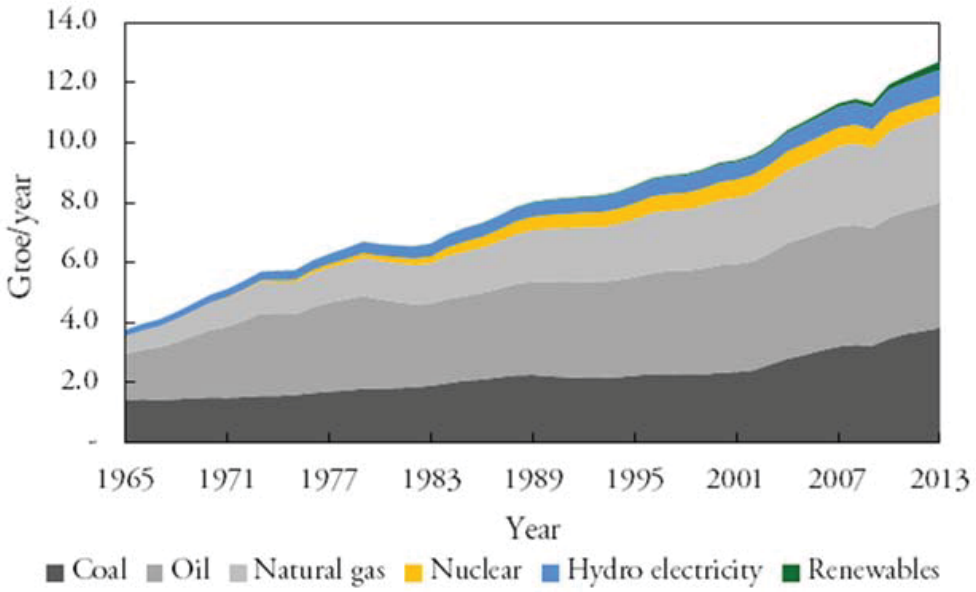


Figure 1.1. Annual total world energy consumption by source [1].

This thesis focuses on thermal radiation within the field of combustion. It is the dominant form of heat transfer in most industrial furnaces [3]. In the improvement and development of new combustion technologies it is therefore important to consider thermal radiation. Computational fluid dynamics (CFD) packages or codes are commonly adopted design tools for combustion applications. In combustion environments the CFD codes solve simultaneous transport models for chemical reactions, flow, and energy. The transport of thermal radiation is part of the energy transport. All the physical phenomena taking place in a combustion process affect each other. Models are used to describe the different transport phenomena. For thermal radiation models

for the transport of thermal radiation and models for properties of the media, gases and particles, are needed.

## 1.1 Research objectives

The objectives of this study can be divided into two major parts. One part concerns the radiative property models for the gases and particles in combustion environments. The second part is the study of thermal radiation in certain combustion applications.

For the radiative property models the objective is to evaluate, improve, and suggest models that are practical to use for engineering purposes. Very often both gases and particles are found in combustions devices. When particles are found together with gases it can pave the way for simpler gas property models as the particles start to dominate absorption and emission of thermal radiation.

Two combustion applications were studied. The first application was the environment found in gasifiers. The objective was to study the importance of the species CO for thermal radiation in this type of application as very high concentrations of CO exist in these types of environments. The second application was the grate fired furnace combustion technology. For this application the main objective was to study the importance of particle radiation, both numerically and by carrying out measurements.

## 1.2 Methodology

The transport of thermal radiation was considered in this study, but no other physical phenomena. In such for the computational domain the temperature, gas mole fraction, and particle data are always assigned beforehand. Boundary temperatures and emissivities are also preselected.

To evaluate the radiative property models, 1-D combustion-like environments were used in most cases where the simpler engineering models were benchmarked with more advanced models. 3-D environments were also used in some cases but without any benchmarking models.

3-D models were used in the study of thermal radiation in grate fired furnaces. The commercial software ANSYS FLUENT 14.0 was used for the solution of the radiative transport. Two approaches were used in the study of thermal radiation in the grate fired furnace. One used a simple geometry to resembling the grate fired furnace and implemented approximated parameters. The second approach used parameters that were taken from measurements.

## 1.3 Thesis outline

Chapter 2 starts with a general introduction to thermal radiation providing some of the definitions and terminology that are used for describing thermal radiation. This is followed by the description of radiative transport, the radiative transport equation. After this, a section is

devoted to solutions to the radiative transfer equation. Chapter 3 starts with an introduction to radiative properties of gases followed by the theory behind the gas property models applied in this work. The last section in this chapter shows how gas property models are applied in this work. Chapter 4 follows the same structure as chapter 3 but for particle radiative properties. Chapter 5 concerns the modelling and measurement work carried out on grate fired furnaces. Chapter 6 presents the results from the investigations. It starts with the results from the 1-D cases, followed by 3-D cases and ends with the modelling and measurement results related to a 400 kW grate fired furnace. The last chapter, chapter 7, presents the conclusions and future outlook.

# 2 Thermal radiation

Thermal radiation is the heat transfer process that does not need any medium. It is the heat you feel on your face on a sunny day or the heat reaching your cold hands when you warm them in front of the fireplace. Though thermal radiation needs no transfer medium it can still interact with one. The greenhouse effect is one of the more well-known phenomena whereby thermal radiation from different sources, the sun and the earth, interact with the atmosphere. The major part of the thermal radiation, which comes from the sun, is transferred through the atmosphere heating up the earth. At the same time the earth is transferring thermal radiation back into space. Some of the thermal radiation from the earth interacts with gases in the atmosphere and is re-radiated into the lower atmosphere and back to the surface. Because of this effect we have a pleasant average temperature on earth which otherwise would be far below the freezing point, on average. Combustion is another process where the media instead gives rise to thermal radiation. These media, being combustion gases and usually also particles, are at higher temperatures and are therefore the emitting source. The transfer of thermal radiation in combustion devices and how it interacts with the media will be treated herein. This chapter will give an introduction to thermal radiation and important definitions and relations to describe it. It will also describe how the transfer of thermal radiation is mathematically formulated and the models that are used in this work to approximate this complex transfer process.

## 2.1 Introduction to thermal radiation

Thermal radiation comprises electromagnetic waves and is defined as the radiation energy that is emitted specifically because of the temperature of a medium or a body. Radiation can also be described as massless energy quanta, a photon. In the electromagnetic spectrum thermal radiation covers part of the ultra violet, the visible, and part of the infrared spectrum. It is recognised to be found at wavelengths between 0.1-100 μm. In figure 2.1 the thermal radiative spectrum is presented together with other commonly known spectra, within part of the electromagnetic spectrum. The energy of an electromagnetic wave is known to be inversely proportional to its wavelength. To describe thermal radiative energy interactions for a body or medium a few definitions and relations are needed.

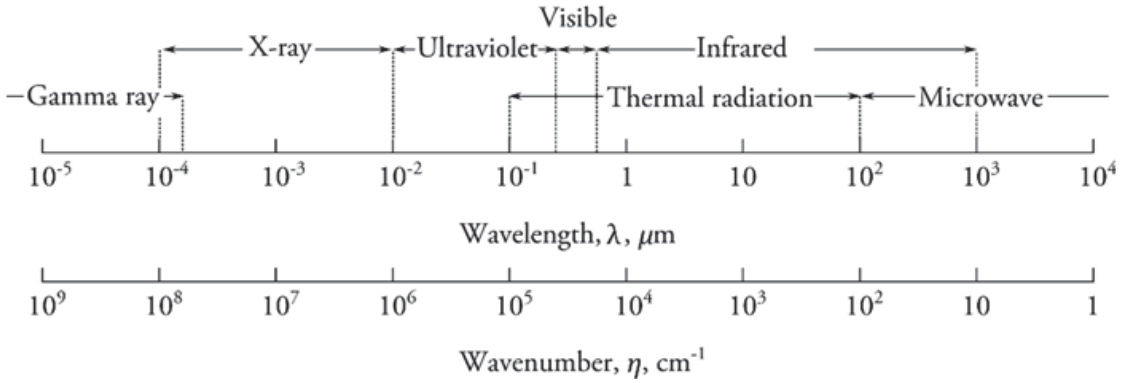


Figure 2.1. Common spectra within part of the electromagnetic spectrum.

## 2.2 Definitions and terminology

This section introduces the definitions, terminology, relations and laws that are needed to describe thermal radiation. Not all definitions of thermal radiation will be given but only those relevant to combustion environments. First, the concept of blackbody will be explained which describes the maximum emissive power of an object or a medium over the spectrum. Second, a description of how thermal radiation can interact with a surface or a medium will be given. Finally, some useful terms are provided. These are needed to describe the transport of thermal radiation.

### 2.2.1 Blackbody radiation

All bodies with a temperature above absolute zero emits radiation. The maximum radiation that can leave a body is blackbody radiation. It therefore serves as a reference for other bodies that can never be truly black over the entire thermal spectrum. The idea of blackbody radiation comes from the visible range within the electromagnetic spectrum. An object appears black to the human eye because it does not reflect any visible light. When an object does not reflect or transmit any radiation incident upon it the object is a perfect absorber, absorbing all radiation. This way of describing the blackbody has been adopted for the entire thermal spectrum. A blackbody is an object that is a perfect absorber at all wavelengths. When an object is a perfect absorber it can be shown by *Kirchoff's law* that it can also be a perfect emitter. To be a blackbody it absorbs all radiation independent of incident direction and emits equally strong radiation in all directions. It was Max Planck [4] who first published work on the blackbody spectral distribution from quantum mechanics. His work is now known as *Planck's law* and presents the spectral emissive power of a blackbody as only being dependent on the temperature, $T$, of the body, for a constant refractive index $n$, as

$$E_{b\lambda} = \frac{2\pi h c_0^2}{n^2 \lambda^5 (e^{hc_0/nkT} - 1)}, \tag{2.1}$$

where λ is the wavelength, $h$ is the Planck constant, $c_0$ is speed of light, and $k$ is the Boltzmann constant. The higher the temperature is of the blackbody, the higher the emissive power, as illustrated in figure 2.2 for a number of temperatures. It can be seen in figure 2.2 that the maximum spectral emissive power goes towards lower wavelengths with increasing temperature of the blackbody. This was shown by Wien [5], prior to the work of Planck, in *Wien's displacement law*.

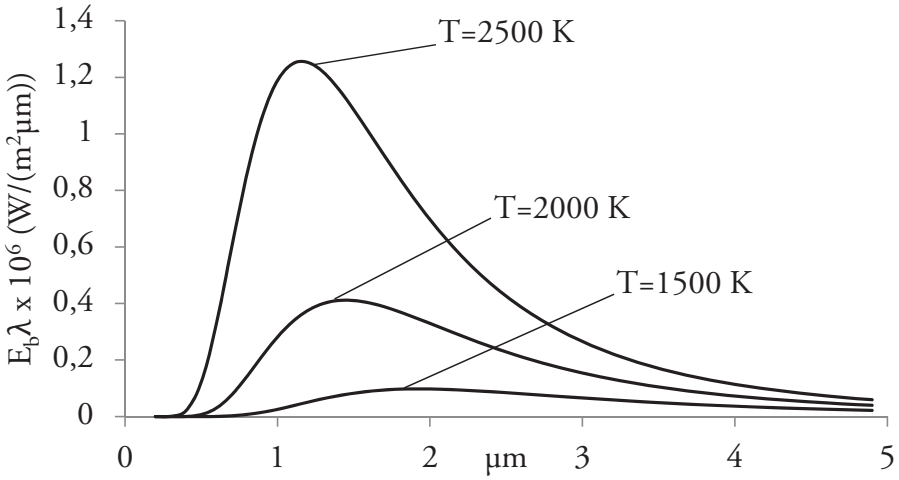


Figure 2.2. The blackbody emissive power at three temperatures.

The total blackbody emissive power is found by integrating equation 2.1 with the whole spectrum, which results in equation 2.2, where σ is Stefan-Boltzmann constant. This is the well-known expression for radiative energy, known as the *Stefan-Boltzmann law*, which shows that the emissive power scales with the temperature to the power of four.

$$E_b(T) = n^2 \sigma T^4 \tag{2.2}$$

## 2.2.2 Interactions with a surface or medium

In the presentation of the blackbody a few of the concepts that describe the interaction between a body and incident radiation upon it have already been presented. Three distinct phenomena can occur for the incident radiation upon a surface: absorption, reflection, and transmission Absorptivity, $\alpha$, the reflectivity, $\rho$, and the transmissivity, $\tau$, are defined to describe the surface properties. Because of the conservation of energy the sum of the absorbed, reflected, and transmitted energy is always equal to the incident radiative energy, $\alpha+\rho+\tau=1$. A surface that is not transmitting any radiation is called an opaque surface. For such a surface the incident radiation is either absorbed or reflected, $\alpha+\rho=1$. The surface properties can be dependent on wavelength, incident direction, and temperature alike. If no comment made regarding the specific surface property it is often the full spectrum hemispherical property that is given. Special

attention needs to be paid to reflectivity; as this property can depend on both incident direction and reflected direction, it is said to be a bi-directional property. In this work it is assumed that all incident radiation upon a surface is reflected equally in all directions; the surface is termed a diffuse reflector. If the incident angle equals the reflected angle the reflection is specular. For a true surface, incident radiation from a certain directions is reflected in all directions with different fractions of the incident radiation energy. More information about surface properties is given by Modest [6].

Emissivity, $\varepsilon$, is another property of a body (surface) or a medium. It describes the ratio of emitted radiative energy to that of a corresponding blackbody with the same temperature. Emissivity takes on a value between zero and one. A surface that has a value below one is called a gray surface. The emissivity of a surface can also have a spectral and directional nature like the other properties. The surfaces in this work will be considered to be opaque. This means that transmissivity does not take place and the emissivity, absorptivity, and reflectivity of surface needs to be determined. Assuming the emissivity to be equal to the absorptivity, according to *Kirchhoff's law*, all properties of the surface can be determined by finding either the emissivity or the absorptivity as $\varepsilon=\alpha=1-\rho$. The main problem with applying *Kirchhoff's law* is that the emission and absorption are stated to be equal for a body in thermal equilibrium with its surroundings. This means that the temperature of the source of radiation, which determines the absorptivity, has the same temperature as the body, which determines the emissivity. This is usually not the case with several surfaces inside combustion environments. The simplified treatment of the surface properties with *Kirchhoff's law* is usually applied in combustion environments and has also been adopted in this work.

Emissivity or transmissivity is often used to describe a participating medium. The transmissivity of a purely absorbing medium can be described by equation 2.3 below. This is known as *Beer-Lambert's law*. Incident radiation upon a medium that is purely absorbing follows an exponential decay which is determined by the distance travelled in the medium, $s$, and the absorption coefficient, $\kappa$, of the medium. The medium can consist of particles and gases. The absorption coefficient is highly dependent on the spectral position, especially for gases. Normally, emission and other types of interactions can take place between an electromagnetic wave and the participating medium. The thermal radiative properties needed to describe these phenomena will be described in upcoming chapters on gases and particles.

$$\tau = 1 - \varepsilon = e^{-\kappa s} \tag{2.3}$$

### 2.2.3 Transport of thermal radiation

To describe the transport of thermal radiation two concept need to be introduced. To describe the directional nature of radiation the concept of the solid angle is used. The emissive power of a body or a medium has directional dependence and the thermal radiative intensity is introduced to account for this.

The solid angle describes how large an object appears to an observer at a certain point. When a unit sphere is placed around the observer the solid angle of the object equals the ratio of the area projected onto the unit sphere to the total area of the sphere, $4\pi$. The solid angle is expressed by the unit steradian, *sr*, where 1 sr=$1/4\pi$. The total solid angle can be expressed by the infinitesimal solid angle in spherical coordinates for the unit sphere as

$$\int_{4\pi} d\Omega = \int_{\varphi=0}^{2\pi} \int_{\theta=0}^{\pi} \sin\theta d\theta d\varphi = 4\pi \tag{2.4}$$

where $\theta$ is the polar angle and $\varphi$ is the azimuthal angle. For a surface the total solid angle becomes that of a hemisphere, which is equal to $2\pi$. For a one dimensional situation, which has been considered in many of investigations described in this work, the hemisphere becomes a half unit circle where the total solid angle equals $\pi$.

The spectral intensity is the flow of radiative energy per unit solid angle, unit time, unit area normal to the direction of interest, and spectral unit. In combustion environments and most heat transfer applications the dependence of time can be neglected. The total intensity reaching a surface, which is known as irradiation, has been investigated in this work, both experimentally and numerically. The total irradiation is expressed by the intensity reaching the surface at a location, $\boldsymbol{r}$, from all directions over a hemisphere

$$H(\boldsymbol{r}) = \int_{0}^{\infty} \int_{2\pi} I(\boldsymbol{r}, \hat{s}_i, \eta) \cos\theta_i d\Omega_i d\eta \tag{2.5}$$

## 2.3 The radiative transfer equation

As noted earlier, when thermal radiation travels through a medium that is only absorbing its attenuation can be described by *Beer-Lambert's law*. For thermal radiation travelling through a medium other types of interactions can also take place such as emission and scattering by the medium. When the medium interacts with thermal radiation one talks about a participating medium.

To describe the radiative transfer through a participating medium one uses the radiative transfer equation (RTE) which can be based on a radiative energy balance over a small volume element. The radiative intensity is used in the RTE being a function of location, $\boldsymbol{r}$, direction, $\hat{s}$, and wavenumber, $\eta$. Before the first order integro-differential equation, which is what the RTE is, is presented, a more generic and illustrative approach with the aid of figure 2.3, is used to describe the RTE. For a small pencil of rays incident on the small volume element with a participating medium, $dV$, in the direction, $\hat{s}$, into the solid angle $d\Omega$, four processes can take place along path $s$. The radiation can be attenuated by absorption (1) or augmented by emission (2), both these processes are related to the absorption coefficient of the medium, $\kappa_\eta$. Scattering can attenuate the radiation by out-scattering (3) or augment it by in-scattering. Both scattering processes are related to the scattering coefficient, $\sigma_{s\eta}$. The in-scattering from a solid angle, $d\Omega_i$, into the solid angle of interest, $d\Omega$, is related to the scattering phase function, $\Phi(\hat{s}_i, \hat{s})$. The scattering phase function gives the probability of the intensity from direction $\hat{s}_i$ to be scattered in the direction of interest, $\hat{s}$.

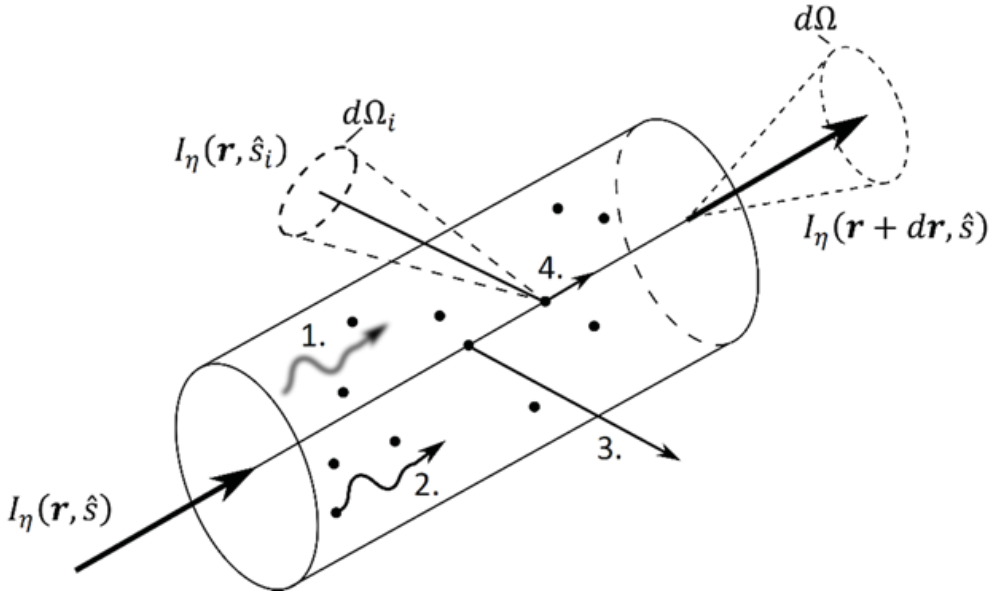


Figure 2.3. Attenuation and augmentation of radiation in a small volume element.

For a participating medium that is non-moving, compared with the speed of light and has a constant refractive index, the RTE, after summing the different attenuations and augmentations and carrying out some mathematical manipulations [6], can be expressed by equation 2.6, where $I_{b\eta}$ is the blackbody intensity.

$$\frac{\partial I_\eta(\boldsymbol{r}, \hat{s})}{\partial s} = \kappa_\eta I_{b\eta}(\boldsymbol{r}) - \kappa_\eta I_\eta(\boldsymbol{r}, \hat{s}) - \sigma_{s\eta} I_\eta(\boldsymbol{r}, \hat{s}) + \frac{\sigma_{s\eta}}{4\pi} \int_{4\pi} I_\eta(\boldsymbol{r}, \hat{s}_i) \Phi_\eta(\hat{s}_i, \hat{s}) \mathrm{d}\Omega_i. \qquad (2.6)$$

To solve the RTE the incoming intensity needs to be specified at some a point. These points are normally the surfaces surrounding the participating medium. For diffusively emitting and reflecting opaque surfaces or walls the intensity leaving a wall in a certain direction can be expressed as,

$$I_{w,\eta}(\hat{s}) = \varepsilon_w I_{b\eta} + \frac{1-\varepsilon_w}{\pi} \int_{\hat{n}\cdot\hat{s}_j<0} I_\eta \left|\hat{n}\cdot\hat{s}_j\right| d\Omega_i \tag{2.7}$$

where $w$, indicates the wall, $\varepsilon$ is the emissivity of the wall, $\hat{n}$ is the normal vector outward the wall, and $\hat{n}\cdot\hat{s}_j$ is the cosine of the angle between the incoming direction and the wall normal. The total radiative heat flux is found by integrating over all directions and over the whole spectrum. The total radiative heat flux to the walls is of great interest in the design of furnaces and other combustion applications. The divergence of radiative heat flux, also known as radiative power and radiative source/sink, is also of interest as it connects the radiate transfer with the overall conservation of energy. From equation 2.6 it can be shown that the total divergence of radiative heat flux can be expressed over a small volume according to equation 2.8 [6]. The first term in equation 2.8, on the right hand side, is from emission. This term increases the source term, which leads to a loss in the overall energy balance. The second term describes the absorption. This term decreases the source term, which leads to a gain in the overall energy balance.

$$\nabla q = \int_0^\infty \kappa_\eta \left( 4\pi I_{b\eta} - \int_{4\pi} I_\eta d\Omega \right) d\eta \tag{2.8}$$

## 2.4 Methods for solving the radiative transfer equation

Solutions to the RTE are generally carried out with some kind of approximate method. Because of the RTEs spatial, directional and spectral dependence, however, exact numerical or analytical solutions can only be found for some special cases, such as plane-parallel environments. Many approximate methods exist. Depending on the purpose of the study and the prevailing conditions different solutions are more or less suitable for solving the RTE accurately. A short introduction is given below to the different approximate methods that are suitable for combustion applications. A review of the different methods for solving the RTE in combustions systems was carried out by Viskanta [7]. He divided the relevant methods for optically self-absorbing situations in combustions systems into four sub-categories, see figure 2.4 below. The optically thin and thick treatment are simple approximations [6] which can give large errors in solutions of radiative transfer in combustion applications [8]. Of the different methods given in figure 2.4, the $P_1$-approximation, the discrete ordinate method (DOM), the discrete transfer method (DTM), and the finite volume method (FVM) are compatible with solutions of other

transport phenomena in CFD environments. The $P_1$-approxiamtion is a spherical harmonics method. The intensity in this method is connected with spherical harmonics related to the Legendre functions for angular variations. A review of the $P_1$-approximation and higher-order approximations can be found in Modest [6]. The discrete ordinates method, also known as the $S_N$-method, is based on a discrete representation of directional intensity. The DOM is used in this thesis and will be described later. The DTRM is a form of ray tracing method that was first introduced by Lockwood and Shaw [9]. The domain is divided into a number of surface elements and volume elements. A selected number of rays are emitted from the surface elements and traced through the volume cells with interactions in each cell. The finite volume method has many similarities with the DOM. Instead of using an angular quadrature scheme, which the DOM use, a finite volume method is used for the direction. Unlike the DOM, the FVM imposes conservation of radiative energy. The method was first introduced by Raithby and Chui [10], more information on the FVM can be found in Modest [6].

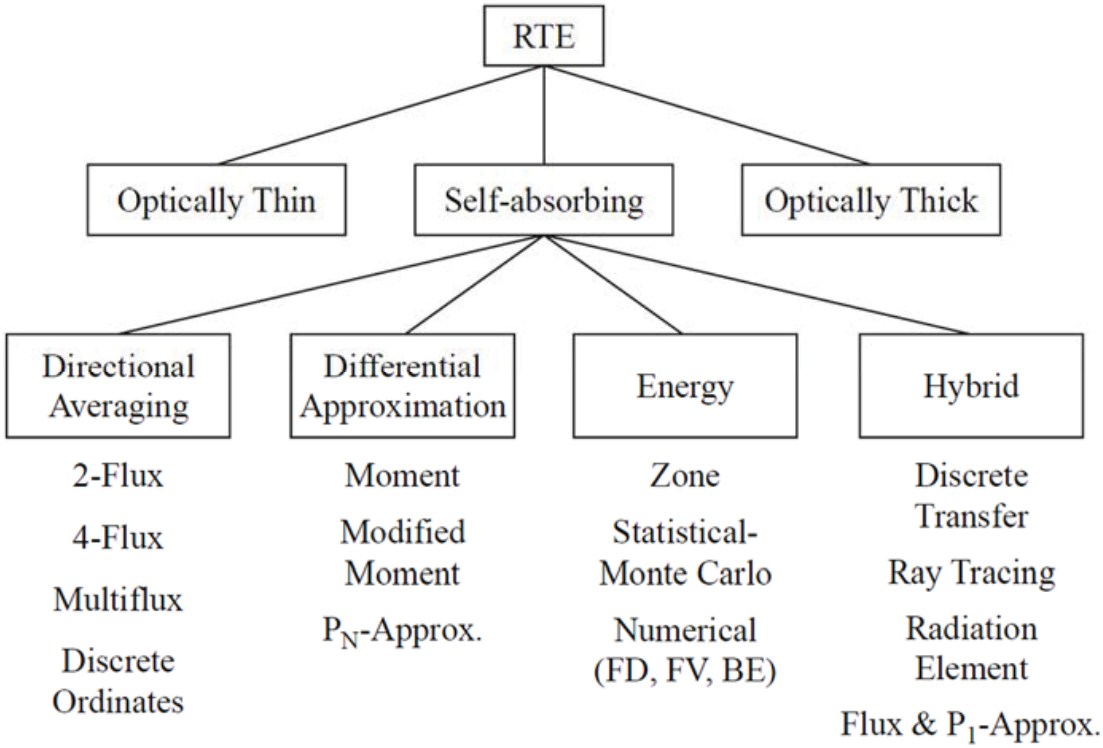


Figure 2.4. Solution methods for the RTE [7].

The first solution of the RTE in this work involved a single radiation path without scattering, as presented in paper I. The radiative transfer along the path was solved together with the transmissivity-based statistical narrow band model, which will be described in chapter 3.5.2. The intensity of a narrow band, $\Delta\eta$, along a discretised radiation path, based on the transmissivity, $\bar{\tau}$, is then expressed as

$$\bar{I}_{\Delta\eta,n} = \bar{I}_{0,\Delta\eta}\bar{\tau}_{\Delta\eta,0\to n} + \sum_{xi=0}^{n-1}\left(\bar{\tau}_{\Delta\eta,xi+1\to n} - \bar{\tau}_{\Delta\eta,xi\to n}\right)\bar{I}_{b,\Delta\eta,xi+1/2}, \tag{2.9}$$

where $n$ marks the endpoint of the last cell along the path 0→n, $xi$ marks the cell boundary positions, and $\bar{I}_b$ is the blackbody intensity for each narrow band. As the considered radiation paths in paper I start from cold surfaces, T=0 K, the first term on the right-hand side of equation 2.9 disappears. The majority of the radiative studies were carried out in plane-parallel environments solving radiative transfer with the discrete ordinates method. 3-D cases were also studied with a radiative solver, the DO-method in the commercial software ANSYS FLUENT 14.0. For more information on the DO-method the reader is referred to the user manuals of the commercial software. The DOM applied to the plane-parallel environment will first be described for absorption-based models and then for transmissivity-based models.

The discrete ordinate method originated from the work carried out by Chandrasekhar [11]. The DOM describes the directional nature of radiation by dividing the total solid angle into a number of discrete directions or ordinates. The radiative transfer is then solved for each direction with a finite difference or finite volume scheme. To find the heat flux and source term the intensity is summed over the total solid angle by means of a numerical quadrature scheme. The RTE, equation 2.6, is approximated for a number of directions, $\hat{s}_i$, dropping the spectral dependence, as

$$\hat{s}_i\frac{\partial I(\boldsymbol{r},\hat{\boldsymbol{s}}_i)}{\partial s} = \kappa(\boldsymbol{r})I_b - \beta(\boldsymbol{r})I(\boldsymbol{r},\hat{s}_i) + \frac{\sigma_s}{4\pi}\sum_{j=1}^{n} w_j I\left(\boldsymbol{r},\hat{s}_j\right)\Phi\left(\boldsymbol{r},\hat{\mathrm{s}}_\mathrm{i},\hat{\mathrm{s}}_\mathrm{j}\right), \quad i = 1,2,\dots,n, \tag{2.10}$$

where $w_j$ is the quadrature weights of the different directions and $n$ is the number of directions. The quadrature weights are used in the numerical quadrature to replace the integral over directions. For first-order linear partial differential equations, as in equation 2.10, one boundary conditions is needed for each direction. For the boundary condition of each direction numerical weights are introduced to replace the integral in equation 2.6 and the wall intensity for a direction is expressed as in equation 2.11. The selection of directions, $\hat{s}_i$, and weights has an effect on the accuracy of the discrete ordinates method. The sets of directions and weights found in the literature often fulfil a number of moments [6]. The DOM is also known as the $S_N$-approximation. $N$ stands for the number of direction cosines found for each principal direction. Each direction is expressed by the direction cosines according to equation 2.12, where $\hat{\imath},\hat{\jmath},\hat{k}$ are the three principal directions of the surface normal, $\hat{n}$. The total number of directions to be considered is related to the number of direction cosines as n=N(N+2).

$$I(\boldsymbol{r}_w, \hat{s}_i) = \varepsilon(\boldsymbol{r}_w) I_b + \frac{1-\varepsilon(\boldsymbol{r}_w)}{\pi} \sum_{\hat{n}\cdot\hat{s}_j<0} w_j I(\boldsymbol{r}_w, \hat{s}_j)|\hat{n}\cdot\hat{s}_j|, \quad \hat{n}\cdot\hat{s}_i > 0 \tag{2.11}$$

$$\hat{s}_i = \xi_i \hat{\imath} + \eta_i \hat{\jmath} + \mu_i \hat{k} \tag{2.12}$$

In this work the $S_8$ – approximation has been used with the weights and direction cosines developed by Fiveland [12]. Several different quadrature are described in the literature. Many of them are mentioned in a study of new quadrature sets by Mishra et al. [13]. In their study the quadrature sets of Fiveland were used and compared. For the plane-parallel environment only one directional cosine is needed, $\mu_i$. For non-scattering cases in the plane-parallel environment only four out of the eight directions needs to be considered because of symmetry between the directions. For the plane-parallel environment equation 2.10 is expressed along the direction $\mu_i$ as

$$\mu_i \frac{\partial I_i}{\partial x} = S_i - \beta I_i, \qquad i = 1,2,\dots,n, \tag{2.13}$$

$$S_i = \kappa I_b + \frac{\sigma_s}{4\pi} \sum_{\substack{j=1 \\ j\neq i}}^{n} w_j I_j \Phi_{ji} \tag{2.14}$$

The phase function in equation 2.14 is normalised as

$$\frac{1}{4\pi} \sum_{\substack{j=1 \\ j\neq i}}^{n} w_j \Phi_{ji} = 1. \tag{2.15}$$

A spatial discretisation is performed for each direction, $\mu_i$, along homogeneous and isothermal cells. With a finite volume scheme, leaving out a few of the derivation steps, the intensity in each cell along a path for the plane parallel environment, with a *step-scheme*, can be expressed as

$$I_{i,xi+1/2} = \frac{S_{i,xi+1/2}(\Delta x) + |\mu_i| I_{i,xi}}{\beta(\Delta x) + |\mu_i|}, \qquad i = 1,2,\dots,n, \tag{2.16}$$

For each direction the iteration starts from the wall where the intensity is known and moves along the cells to the opposite wall. For non-black surfaces and scattering the procedure for finding all intensities is an iterative one. Once all the intensities are found the wall radiative heat flux and source term in a cell are calculated by

$$q(\boldsymbol{r}_w) \simeq \varepsilon(\boldsymbol{r}_w)\pi I_b - \varepsilon(\boldsymbol{r}_w) \sum_{\hat{n}\cdot\hat{s}_i<0} w_i I(\boldsymbol{r}_w, \hat{s}_i)|\hat{n}\cdot\hat{s}_i|\,, \tag{2.17}$$

$$\nabla q = \kappa\left(4\pi I_b - \sum_{i=1}^{n} w_i I(\hat{s}_i)\right). \tag{2.18}$$

For narrow band models the DOM approach suggested by Kim et al. [14] is implemented. The intensities are then found at the boundaries of the cells. The intensity is then discretised along a path, dropping the spectral dependence, as

$$\bar{I}_{i,xi+1} = \bar{I}_{i,xi} + \left(1 - \bar{\tau}_{i,xi\to xi+1}\right)\bar{I}_{b,xi+1/2} + \bar{I}_{w,xi}\left(\bar{\tau}_{i,w\to xi+1} - \bar{\tau}_{i,xi\to xi}\right) + \bar{C}_{i,xi+1/2}, \tag{2.19}$$

$$\bar{C}_{i,xi+1/2} = \sum_{k=1}^{xi-1}\left[\left(\bar{\tau}_{i,k+1\to xi+1} - \bar{\tau}_{i,k+1\to xi}\right) - \left(\bar{\tau}_{i,k\to xi+1} - \bar{\tau}_{i,k\to xi}\right)\right]\bar{I}_{b,k+1/2}. \tag{2.20}$$

The radiative source term is for the transmissivity-based models, in the plane-parallel cases, given by equation 2.21. The method for solving of the intensity, as in equation 2.19 and 2.20, use the correlated approach for an intensity path based on transmissivity, as in equation 2.9. In this approach, depending on the spatial and directional discretisation, a large number of transmissivities need to be pre-calculated before intensities within each narrow band are calculated. A non-correlated approach has also been investigated which can significantly speed up the solution of the RTE with the narrow band model. More on this approach and how to determine the transmissivity for a narrow band model are described in chapter 3.

$$\nabla q = \frac{q_{xi} - q_{xi-1}}{x_i - x_{i-1}}. \tag{2.21}$$

There are two problems with the DOM. The ray effect is one of them. It is a product of angular discretisation. Ray effects decrease with the number of directions but can never disappear. Lee et al. [15] gave a good description of ray effects. A second problem is false scattering. As radiation travels through an enclosure a type of broadening takes place because of the way the DOM functions. This behaviour results in non-physical smearing of the radiation and can be lessened by using an increased number of cells in the considered domain.

The DOM accuracy has been investigated in several previous studies. Sing et al. [16] compared the DOM, DTM and FVM for plane-parallel geometries with absorbing/emitting and scattering media. They conclude that when the same quadrature schemes are used for all models the accuracy of the different models compares very well. The FVM and DOM were compared

with exact models in 3-D geometries by Kim et al. [17]. They also concluded that the models compared well, but that the FVM performed better in optically thin media.

# 3 Gas radiative property models

This chapter deals with the gas radiative property models that have been used in this thesis: line-by-line calculations, statistical narrow band models, and weighted sum of gray gas models. The chapter starts with an introduction to how radiation interacts with molecular gases, followed by three sections describing the property models, and ending with a section that describes how the models are applied. Short descriptions of other property models are also given.

## 3.1 Interaction of thermal radiation with molecular gases

When thermal radiation travels through a molecular gas it can be either absorbed or transmitted. The molecule can also emit thermal radiation by either spontaneous or induced emission. Scattering can also occur between an electromagnetic wave and a molecule but is not relevant in the case of thermal radiation [6]. If an interaction between an electromagnetic wave and a molecule takes place the energy of the wave must match the energy of the molecule. The energy of an electromagnetic wave is inversely proportional to its wavelength. The energy of a molecule, relevant in combustion applications, is related to the rotation and vibration of the molecule. An example of rotation and vibration by a $CO_2$ molecule is provided in figure 3.1. The different rotational and vibrational transitions of the molecule are related to certain energy levels that form a large number of lines in the thermal radiative spectrum. The vibrational transitions require more energy than rotational transitions. Also, rotational transitions are practically always accompanied by vibrational transitions. Therefore these two transitions form closely packed lines in the spectrum called vibration-rotation bands. As regards the molecular species investigated in this thesis the relevant vibration-rotation bands for $H_2O$ are found at 6.3, 2.7, 1.87, and 1.38 μm, for $CO_2$ at 4.3, 2.7 and 2.0 μm and for CO at 4.7 μm. The lines are not found in discrete positions in the spectrum but are broadened due to so-called broadening effects. The broadening relevant to combustion, in most cases, is collision broadening, caused by collisions of molecules. Other broadening effects are natural broadening and Doppler broadening [6].

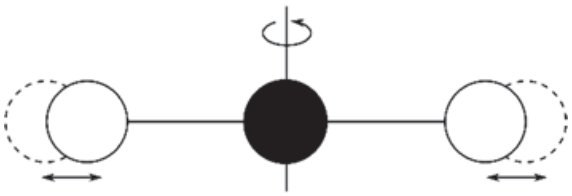

Figure 3.1. Illustration of rotation and vibration by $CO_2$.

## 3.2 Line-by-line calculations

Line-by-line (LBL) calculations use high resolution spectral databases to calculate the spectral absorption coefficient. The LBL approach is considered to be the most accurate method for describing the absorption coefficient and is often used to benchmark simpler models. LBL calculations use spectral parameters from spectral databases to generate the important transition lines. LBL calculations have been around since the 1960s, originally for applications of atmospheric calculations. The spectral absorption coefficient for a molecular specie at a wavenumber, $\eta$, is summed over all transition lines contributing to that specific spectral position as

$$\kappa_\eta = N \sum_k S_k(T) f_k(\eta), \tag{3.1}$$

where $N$ is the molecular mole density of the specie, $S_k$ is the integrated line intensity for the line $k$, also known as line strength, and $f_k$ is the line shape profile. The molecular mole density of a specie is derived from the equations of state and given by

$$N = \frac{A_v}{RT} xP \tag{3.2}$$

where $A_v$ is the Avogadro constant, $R$, is the universal gas constant, $x$ is the specie mole fraction, and $P$ is the total pressure. The line strength is dependent on temperature, $T$, and is given by scaling the line strength from the reference temperature, $T_0 = 296$ K as,

$$S_k(T) = S_k(T_0) \frac{Q(T_0)}{Q(T)} \frac{1 - \exp(-C_2\eta_k/T)}{1 - \exp(-C_2\eta_k/T_0)} \exp\left( C_2 E'' \left( \frac{1}{T_0} - \frac{1}{T} \right) \right), \tag{3.3}$$

where $Q$ is the partition function, $C_2$ is the second Planck constant, $E''$ is the lower state energy, and $\eta_k$ is the energy difference between the initial and final state. The partition function, $Q(T)$, also known as the total internal partition sums, in relation to thermal radiation is the sum of all rotational and vibrational energy levels of a molecule for a specific temperature. The partition function is the product of rotational and vibrational partition functions. The partition function is a very complex function that can be derived from quantum mechanics or found by using calculated tabulated data, such as those supplied by Fischer et al. [18] for temperatures between 70-3000 K. In this thesis a rigid-rotator, harmonic-oscillator model was used to describe the rotational-vibrational partition function [19]. The ratio of the partition functions, as in equation 3.3, is given by

$$\frac{Q(T_0)}{Q(T)} = \left( \frac{T_0}{T} \right)^n \frac{\prod_i (1 - \exp(-C_2\eta_i/T))}{\prod_i (1 - \exp(-C_2\eta_i/T_0))} \tag{3.4}$$

where $\eta_i$ is the spectral position of the fundamental vibration band of the molecule and $n$, is a rotational exponent. For linear molecules such as $CO_2$ and CO, n=1, and for non-linear molecules such as $H_2O$, n=1.5. The last parameter in equation 3.1 is the line shape profile, $f_k(\eta)$. For combustion applications with atmospheric pressure equal to or greater than unity and temperatures under 2000 K collision broadening dominates the broadening of the spectral lines [6]. Therefore the line shape profile follows the Lorentz profile,

$$f_k(\eta) = \frac{1}{\pi} \frac{\gamma_k}{\gamma_k^2 + (\eta - \eta_k)^2}, \tag{3.5}$$

where $\gamma_k$ is the pressure broadened line half-width and $\eta_k$ is the wavenumber at the line centre. The pressure broadened line half-width can be expressed as

$$\gamma_k = \left(\frac{T_0}{T}\right)^{n_c} \left[\gamma_{self,k} p_c + (P - p_c)\gamma_{air,k}\right], \tag{3.6}$$

where $n_c$ is a coefficient of temperature dependence, $p_c$ is the partial pressure of the absorbing gas, and $\gamma_{self,\,k}$, $\gamma_{air,\,k}$ are the line self-broadening and air-broadening, respectively [20]. The line parameters $S_k(T)$, $E''$, $\eta_k$, $\gamma_{self,\,k}$, $\gamma_{air,\,k}$, and $n_c$ can be found from spectral databases. For a mixture of species, $i$, the spectral absorption coefficient is defined according to equation 3.7.

$$\kappa_{\eta,mixture} = \sum_i \kappa_{\eta,i} \tag{3.7}$$

Many databases have been developed over the years. For atmospheric calculations, and other applications, the HITRAN molecular spectroscopic database is the standard database, presented first at the beginning of the seventies [21] and in many updated versions after that, the latest one being the HITRAN2012 [22]. For combustion applications and high temperature applications the HITRAN database misses the so-called hot lines. The latest version that accounts for hot lines is the HITEMP2010 database [23]. This database was used for the LBL calculations in this thesis. The number of lines in the database for $H_2O$ and $CO_2$ is 114 million and 11 million, respectively. It was shown in a recent work, investigating a number of combustion-like cases, that the choice of database is important [24]. The authors recommended that the HITEMP2010 should be used for benchmarking other approximate models.

## 3.3 Band models

Band models try to describe the spectral behaviour of a large group of lines within a part of the spectrum. Band models can be divided into two groups depending on their spectral resolution. Narrow band models have a spectral resolution in the order of 10 $cm^{-1}$ whereas wide band

models have a spectral resolution in the order of 100 $cm^{-1}$ and attempt to describe the entire vibration-rotation band. There are three commonly recognised type of narrow band models: the Elsasser model, statistical models and *k*-distribution models. The first was developed by Elsasser [25] and assumed that the lines within the band are equally distributed with equal line strength. Statistical models are based on Goody´s hypothesis [26] that the lines within the band are randomly distributed and line strength is not equal but follows a probability distribution. The narrow band model based on *k*-distribution reorders the absorption coefficient into a smooth continuous function over the band. This reordering of the absorption coefficient was described by Arking and Grossman [27]. The commonly recognised wide band model is the exponential model first developed by Edward and Menard [28]. They suggested that an adequate number of narrow bands within the wide band can be described by simple exponential relations. Statistical narrow band models have been used in this thesis and will be further described.

The spectral resolution of the narrow bands permits averaging of the important parameters that describes the lines and distribution within the band. The smallness of the band also allows for the Planck function to be assumed as constant over the band. Transmissivity is used in statistical narrow band (SNB) models and therefore the average transmissivity for a band is described as

$$\bar{\tau}_{\eta} = exp(-\bar{W}/d) \,, \tag{3.8}$$

where $\bar{W}$ is the average equivalent width of the spectral lines in the band and *d* is the average distance between the lines. If the line strength follows a probability function then the average equivalent line width can be written as,

$$\bar{W} = \int W(S,u)P(S)dS \,, \tag{3.9}$$

where *W* is the equivalent width of a single line, *u* is the optical depth, and *P(S)* is a probability function for the line strength. An exponential probability function was first suggested by Goody [26]. Later, Malkmus [29] suggested an exponential-tailed probability function that accounted for low-intensity lines. The conditions of a Lorentz line shape, as presented in equation 3.5, mean that for an isothermal and homogeneous path the transmissivity for the Goody and Malkmus probability distributions can be described as in equations 3.10 and 3.11, respectively. The two approaches for describing the probability distribution resulted in the SNB models that are today known as the Goody and Malkmus models.

$$\bar{\tau}_{\eta,G} = exp\left(-\frac{\bar{S}}{d}u\left(1+\frac{\bar{S}}{d}\frac{u}{4\bar{\gamma}/d}\right)^{-1/2}\right) \tag{3.10}$$

$$\bar{\tau}_{\eta,M} = exp\left(-2\frac{\bar{\gamma}}{d}\left(\left(1+\frac{\bar{S}}{d}\frac{u}{\bar{\gamma}/d}\right)^{\frac{1}{2}}-1\right)\right) \tag{3.11}$$

In equations 3.10 and 3.11, average line strength to line distance, $\bar{S}/d$, and the average line half- width of Lorentz lines to average line distance, $\bar{\gamma}/d$, are known as the narrow band parameters. The line half-width is dependent on both pressure and temperature whereas $\bar{S}/d$ and *1/d*, known as structure parameters, are only dependent on temperature. The Lorentz line half-width can be found from kinetic theory [6] whereas structure parameters are often tabulated for narrow bands dependent on temperature. The tabulated data were constructed from an anharmonic oscillator/rotator model and from experimental data [30] in the work of Grosshandler [31] and adapted to the Goody model. The tabulated data are used in a computer code named RADCAL [32]. Soufiani et al. [33, 34] created the tabulated data starting off from a spectral databases and used it for the Malkmus model. This database is known as the EM2C database as it was developed by researchers associated with the EM2C laboratory in France. The two SNB models and the different constructed narrow band parameters of [30, 33] were evaluated in the work of Marakis [35] for $H_2O$. By using the same narrow band parameters of [33] he found the smallest discrepancies between the two models but the Malkmus SNB model performs somewhat better. Because of the significantly simpler mathematics of the Goody model Marakis concluded that the Goody model is still useful.

So far a homogeneous and isothermal radiation path has been considered. For thermal radiation paths that are inhomogeneous and/or non-isothermal, narrow band parameters are described for an equivalent uniform path by the Curtis-Godson approximation [36]. The equivalent parameters are defined by equations 3.12-3.14. For a mixture of species, the transmissivity over a radiation path is taken by the product of the individual species' transmissivities [37].

$$u = \int_0^l xPds \tag{3.12}$$

$$\left(\frac{\bar{S}}{d}\right)_{eq} = \frac{1}{u}\int_0^l \frac{\bar{S}}{d}xPds \tag{3.13}$$

$$\left(\frac{\bar{\gamma}}{d}\right)_{eq} = \frac{1}{u}\left(\frac{\bar{S}}{d}\right)_{eq}^{-1}\int_0^l \frac{\bar{\gamma}}{d}\frac{\bar{S}}{d}xPds \tag{3.14}$$

SNB models have been compared and validated against LBL models in a number of works [24, 33, 38]. In most cases the SNB models perform very well, although for highly reflecting walls the SNB can create significant errors [38]. As it is a transmissivity-based model, general solution methods do not allow for scattering from particles [6].

## 3.4 Global models

Global models use parameters to describe the radiative properties over the whole spectrum by correlating them with data found from more advanced models. The global model is therefore also known as a correlation or full spectrum model. The most common global model is the weighted sum of gray gas model (WSGG). The model was first described by Hottel and Sarofim [39], that emissivity can be expressed by a weighted sum of a number of gray gases. An extension of the WSGG model was carried out by Denison and Webb [40]; known as the spectral-line-based weighted sum of gray gas model (SLW). They introduced a new weighting based on the reordered absorption coefficient, an inversed k-distribution over the whole spectrum [41]. This reordering was also adopted in the full spectrum correlated k- distribution (FSK) model [42] and the fictitious gas absorption distribution function (ADF) [43]. The SLW, FSK, and ADF above were the first versions of the models, and improvements have since been made to both the models and the correlated coefficients. The WSGG model has been used in this thesis and will be given more attention in upcoming paragraphs.

The emissivity for a homogeneous column of gas can be expressed with the WSGG model as

$$\varepsilon = \sum_{i=0}^{N_g} a_i(T)(1 - e^{-\kappa_i p_c s}), \tag{3.15}$$

where $N_g$ is the number of gray gases, $a_i(T)$ is the blackbody weights of the $i$-th gray gas, $\kappa_i$ is the gray gas absorption coefficient, $p_c$ is the gas partial pressure of the absorbing gas, and $s$ is the path length. One interpretation of the WSGG parameters is that the blackbody weights corresponds to fractions of blackbody radiation where the absorption coefficient is $\kappa_i$. The implementation of the WSGG in the RTE was demonstrated by Modest [44]. All blackbody weights sum up to unity. To represent the clear parts of the spectrum where no emission/absorption is taking place a clear gas is introduced, $\kappa_i = 0$. The corresponding blackbody weight for the clear gas is defined as

$$a_{i=0} = 1 - \sum_{i=1}^{N_g} a_i \tag{3.16}$$

The blackbody weights and gray gas absorption coefficient are fitted against emissivity data produced at different pressure path-lengths and temperatures. The emissivity data are often

produced from more sophisticated models such as LBL calculations based on spectral databases or narrow band models. In this thesis the HITEMP2010 database together with LBL calculations and the Malkmus SNB model [34] were used to produce the needed emissivity data. Blackbody weights are often produced as a function of temperature. A polynomial function is commonly adopted to fit the blackbody weights. The coefficients are normalised with a reference temperature, $T_{ref}$, as in equation 3.17. In equation 3.17 the value $N_C$ is the number of polynomial coefficients and $c_{i,j}$ is the polynomial fitting coefficients.

$$a_i = \sum_{j=1}^{N_c} c_{i,j} \left( \frac{T}{T_{ref}} \right)^{j-1} \tag{3.17}$$

The WSGG model has been used extensively throughout the literature where new sets of parameters have been produced for several different applications. With $H_2O$ and $CO_2$ being the dominating radiating species WSGG parameters are produced for a certain ratio between the two species´ mole fractions, $x(H_2O)/x(CO_2)$. When the WSGG is adapted to environments where the ratio of mole fractions between the $H_2O$ and $CO_2$ changes, fitting between sets of coefficients can be introduced [45, 46]. The accuracy of the WSGG in predicting radiative heat flux and source term has been evaluated in many works, [38, 45-48]. Many investigations such as that by Goutiere et al. [48] do not make a fair comparison of the WSGG model and the more advanced models, as WSGG parameters are not based on the more advanced models or the same spectral database. The errors in such cases cannot be fully traced as they can belong both to the model and the source with which the parameters are correlated. The more relevant studies reveal that the WSGG model can give reasonable accuracy in prediction of both the heat flux and source term for smooth variation in the temperature field, where the media are hot and the walls are colder. The predictions by the WSGG model are much less accurate for hot walls and cold media and for cases with steep gradients in temperature. The inaccuracies of the WSGG model derive from the fact that it is an emission based model, where the weighting factors are taken for the temperature of the emitting body. Therefore it can give inaccurate representation of gaseous absorption. The WSGG model has been used together with particles in this thesis. That being so, the errors of the gas model are overshadowed by the particles absorption and emission. A gray model based on the WSGG parameters has also been used. The reason for this was to evaluate the gray WSGG-based model, which is commonly used in commercial software, such as ANSYS FLUENT.

## 3.5 Applied modelling approaches

Three models, and versions of them, have been used for determining the radiative properties of gases, LBL calculations, the Goody and Malkmus SNB models, and the WSGG model. This section will describe how the models were applied and in some cases improved. In the previous sections the theory behind the models was described. This section follows the same order.

### 3.5.1 LBL calculations

LBL calculations were used for benchmarking the simpler models and producing emissivity data used for determining the WSGG parameters, in papers III and V. In all cases, where the LBL calculations were applied to benchmark simpler models, plane-parallel environments were used. The RTE was solved with the DOM method, as explained in chapter 2.4. The implemented LBL calculations were validated against the work of Kangwanpongpan et al. [46], figure 3.2.

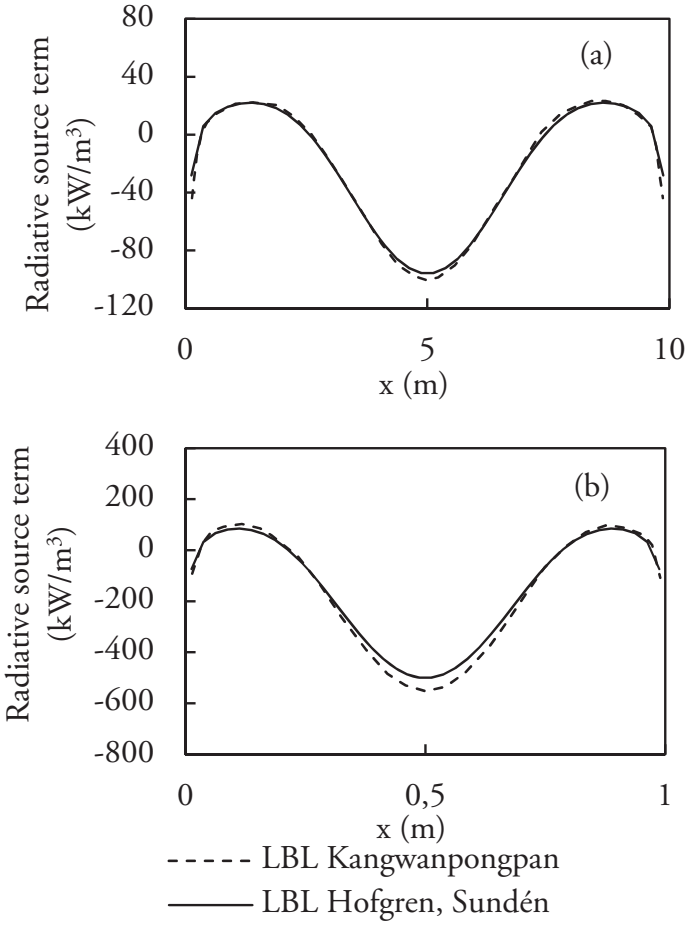


Figure 3.2. Source terms for LBL calculation, present work and [46], model in a plane-parallel non-isothermal environment with a) 10 m. distance, b) 1 m distance; the setup of Fig. 8 (b),(d) in [46] was adopted.

The difference between the models were discussed in paper III. What was not mentioned was the different treatment of the partition function, which could also lead to a difference between the two models. The difference were, however, considered as acceptable for the purpose of the this thesis. The spectral absorption coefficient was determined by LBL calculations in the spectral range of 0.2-10.000 $cm^{-1}$ with a resolution of 0.067 $cm^{-1}$. This resolution was also used by Kangwanpongpan et al. [46]. The selected resolution was found to give good accuracy and speed, keeping the error below 0.1 percent for the heat flux and source term, compared with the

resolution of 0.02 $cm^{-1}$, used by Chu et al. [24]. LBL calculations were used to benchmark the SNB models and the WSGG models. The production of emissivity data for fitting of WSGG parameters is described in section 3.5.3.

### 3.5.2 SNB modelling

SNB models are seen as one of the more promising alternatives to the computationally heavy LBL calculations. However, narrow band calculations are computationally heavy and not suitable for engineering purposes. To make the SNB models less computationally heavy two methods to speed up the model were investigated. By using look-up tables instead of using interpolation of the structure parameters or molecular models one can speed up the SNB calculations. This approach is used, extended, and validated for the CO specie, as shown in paper I. In this study the importance of CO thermal radiation is also investigated for environments with high CO concentrations, such as that found in gasifiers. A non-correlated approach can also be used for solving the radiative transfer along an intensity path, as evaluated in paper VI. The accuracy of the non-correlated approach was investigated for cases with soot present. A gray narrow band (GNB) model based on the non-correlated SNB suggested by Liu et al. [49] was also investigated in paper VI. Cases investigated with SNB models are plane-parallel environments.

The use of look-up table for the structure parameters, $\bar{S}/d$ and *1/d*, was introduced by Yan and Holmstedt [50]. They showed that by using a look-up table that divides the temperature dependence into a resolution of 10 K one can solve the radiative transfer more than 20 times faster with minimal error in the radiative intensity predictions than the methods used in RADCAL [32]. The investigations were carried out for cases with $CO_2$, $H_2O$ and soot. This thesis extended and validated the model for the radiating species CO. It was validated primarily against the experimental work of Abu-Romia and Tien [51] along a homogeneous radiation path containing only CO at two pressures, see figure 3.3. The CO volume fraction can be above 50 percent in some combustion environments such as those in gasifiers. The CO contribution to the total directional radiative heat flux was investigated in this type of environment, in which small volume fractions of $CO_2$ and $H_2O$ were also present.

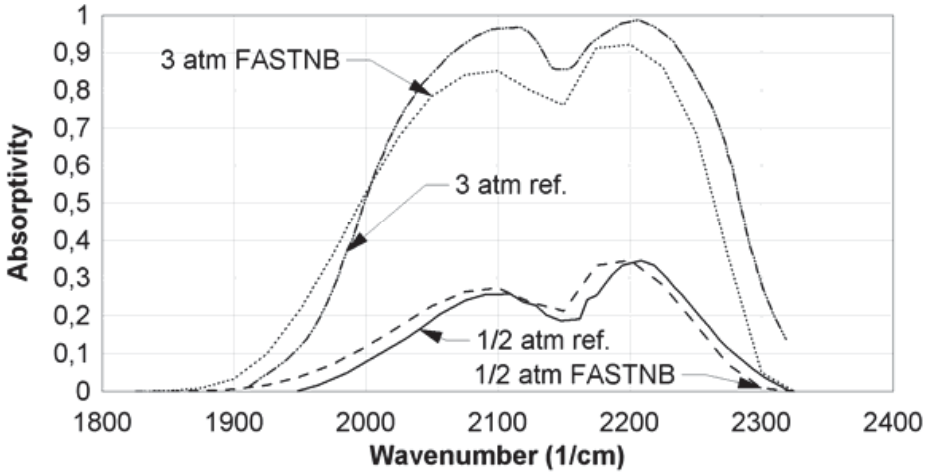


Figure 3.3. Comparison of the absorptivity at the fundamental band of CO through a 20 cm path at 900 K at total pressures of 0.5 and 3 atm. Paper I.

The investigations in paper I were based on the Goody SNB model. The Goody model can give larger errors in its thermal radiation predictions than the Malkmus model. Therefore, continuing work on the SNB model, paper VI, used the Malkmus model and the EM2C database [34], see chapter 3.3. The correlated approach to solving the radiative transfer along an intensity path for a narrow band, $\Delta\eta$, from point *0* to a point *n*, for the transmissivity-based models along a number of homogeneous and isothermal cells was presented in chapter 2, equation 2.9. The summation term in equation 2.9 is what makes the correlated SNB computationally heavy. A non-correlated solution, dropping the spectral dependence between intensity and transmissivity, is given by equation 3.18, solving the intensity from cell to cell.

$$\bar{I}_{\Delta\eta,xi} = \bar{I}_{\Delta\eta,xi-1}\bar{\tau}_{\Delta\eta,xi-1\to xi} + \left(1-\bar{\tau}_{\Delta\eta,xi-1\to xi}\right)\bar{I}_{b,\Delta\eta,xi-1/2}. \tag{3.18}$$

The speed-up with the non-correlated solution scales with the number of cells along a radiation path. The non-correlated SNB has been investigated in several previous studies [35, 49, 52, 53]. Some recognised that the non-correlated approach can give large errors in predicting the radiative transfer. *Yan* [53] used the non-correlated approach and describing it as a true candidate to the correlated SNB in combustion environments, especially when soot was present. Soot impact on the radiative heat flux predictions of the non-correlated SNB was also investigated by Zhang et al. [52], who showed that even with soot the prediction of the non-correlated approach was unsatisfactory. As the non-correlated SNB model can offer a significant speedup of thermal radiative calculations a number of sooty combustion-like environments were investigated for the predictive abilities of the radiative source term and the wall heat flux, paper VI. The gray narrow band model was evaluated together with the non-correlated SNB. An equivalent gray absorption coefficient was calculated from the non-correlated SNB within each

narrow band. The absorption coefficient was given by equation 3.19, where the $L_{MBL}$ is the mean beam length of the local radiation path, Liu et al. [49]. As the GNB is an absorption-based model it is easier to implement it in conventional solution methods for the RTE. The simpler WSGG model was also used and compared with the correlated and non-correlated SNB models in paper VI.

$$\bar{\kappa}_{\Delta\eta,xi+1/2} = \frac{-\ln(\bar{\tau}_{\Delta\eta}\,(L_{MBL})}{L_{MBL}} \tag{3.19}$$

### 3.5.3 WSGG modelling

The WSGG model was used in papers II, III, V, and VI. In all cases it was applied in combustion-like environments where particles also absorbed and emitted radiation. The model was applied in both plane-parallel cases and in 3-D cases.

The WSGG model was first used in paper II with the parameters from Truelove [54]. In this parametric study on the radiative transfer in a grate fired furnace-like environment the WSGG model was used together with absorbing and scattering fly ash and char particles. The WSGG model was applied into the commercial software ANSYS FLUENT 14.0 for solution of the radiative transfer. In papers III, V, and VI new sets of WSGG parameters were produced. In paper III and V the parameters were correlated to emissivity data produced by LBL calculations using the HITEMP2010 database. In paper III the use of Planck mean coefficients for particles was investigated in combustion-like environments. A new approach was investigated whereby the particle absorption coefficient was incorporated into the WSGG model. This approach was compared with the WSGG model together with the Planck mean absorption coefficient for the particles and benchmarked against LBL calculations together with spectral particle properties derived from the Mie theory in plane parallel cases. How the particles were introduce is explained in chapter 4. In paper V the WSGG model and a gray-WSGG model were compared and benchmarked against LBL calculations in plane-parallel cases with soot particles present. The WSGG parameters for the non-gray WSGG model are presented in table 3.1, which was used in papers III and V. The parameters were calculated from emissivity data produced by LBL calculations. More details is provided in the next paragraph. The WSGG model was also investigated in assessment of non-correlated SNB model in sooty plane-parallel environments, paper VI. The WSGG parameters were then produced from the SNB model by the same method used for WSGG parameters produced from LBL calculations. This was to enable fair comparison of the different models. Soot was introduced by extra gray gases or by using the Planck mean coefficient. More about the soot absorption coefficient and how it is applied together with the WSGG model can be found in chapter 4. A gray-WSGG and the non-gray WSGG model, as the models are referred to in paper V, were applied to a real grate fired furnace case. More information on the real grate fired furnace case is given in chapter 5. The gray-

WSGG model is commonly used in commercial softwares, such as ANSYS FLUENT 14.0. The purpose of using the gray-WSGG model is to evaluate its performance when particles are present and when they are not present. A domain-based gray-WSGG model was used with a mean beam length $L_{MBL}$=1.76L, where L was the distance between the planes. The gray absorption coefficient was calculated with equation 2.3, the distance, *s*, being replaced with the mean beam length and an emissivity calculated with equation 3.15. This approach to acquiring the absorption coefficient has no sound theoretical foundation but can still give good estimations of predictions of wall radiative heat flux [55].

Table 3.1. WSGG parameters for water and carbon dioxide at a total pressure of one atmosphere, papers III and V.

| i | $\kappa_i$ *(1/(atm m))* | $c_{i,1}$ | $c_{i,2}$ | $c_{i,3}$ | $c_{i,4}$ | $c_{i,5}$ |
|---|---|---|---|---|---|---|
| $x(H_2O)/x(CO_2)$=1 | | | | | | |
| 1 | 0.412 | 0.1340 | 0.8748 | -1.0000 | 0.5198 | -0.1048 |
| 2 | 5.25 | 0.2142 | 0.2814 | -0.4119 | 0.1384 | -0.0119 |
| 3 | 67.2 | 0.1202 | 0.1089 | -0.3119 | 0.1886 | -0.0365 |
| $x(H_2O)/x(CO_2)$=2 | | | | | | |
| 1 | 0.2753 | 0.1459 | 0.6735 | -0.7741 | 0.4448 | -0.0977 |
| 2 | 3.8729 | 0.1711 | 0.5274 | -0.5788 | 0.1842 | -0.0178 |
| 3 | 48.5893 | 0.1572 | 0.1845 | -0.4945 | 0.2936 | -0.0552 |

The emissivity data from the LBL calculations were produced at 22 temperatures equally spaced between 400-2500 K. 27 pressure path-lengths were used between 0.01-10 bar m. The total pressure was set to 1 bar. Three gray gases and one transparent gas were used. The blackbody weights were fitted against a $4^{th}$ degree polynomial giving rise to five polynomial coefficients, $N_C$ = 5, in equation 3.17. An over-represented system was formed with 18 coefficients to be determined from 594 emissivity values. A least square method was used to minimise the difference between the emissivities of the WSGG model and the LBL calculations. More details on the method for acquiring the WSGG parameters can be found in paper III.

# 4 Radiative properties of particles

In this thesis the properties for different kinds of particles have been applied on a spectral, global, and gray basis in combustion-like environments. This chapter starts by introducing the reader to the type of particles that can be found in combustion environments. A second part describes how radiation interacts with a particle and the parameters needed to describe the particle properties. The two sections following describe the theory behind the spectral models applied in this work. This is followed by a section that explains the gray models that are commonly used in combustion environments. The last section presents how the modelling of particle properties were applied in this work.

## 4.1 Particles in combustion devices

Before describing what the properties of particles are and how to describe them it is important to know what type of particle one can expect in a combustion device. The most commonly found particle in combustion devices is the soot particle. Soot is formed in the fuel-rich regions of the flames as a result of incomplete combustion. Polycyclic aromatic hydrocarbons (PAHs) are acknowledged to be the precursors for the formation of soot [56]. Combustion of volatiles and tars is the key step in the formation of PAH and soot [57]. Soot can be found in sizes ranging from 50 nm to 0.3 µm [6]. In devices combusting solid fuel, particles from fuel, char, and ash can also be found. The type of combustion device and the fuel type have a large impact on where the particles can be found in the furnace. In pulverised combustion devices the fuel and char particles can be found in a large part of the furnace. In fixed-bed combustion most fuel and char particle are found close to the bed. Fuel and char particles leaving the bed do so by entrainment. A large amount of char can be found in the freeboard of fixed-bed furnaces, as shown in paper II. The existence of ash in the combustion device is first and foremost dependent on the amount of mineral matter in the fuel. Ash particles exist inside the combustion device in similarly as for char and fuel particles. Small ash particles are also formed from the gaseous form of the mineral matter in a very complex process of nucleation formation and condensation of species [57, 58]. Sizes of fuel, char, and ash particles can be found from nano-scale up to several hundreds of micro-metres. Which sizes found are dependent on the combustion device, the fuel, treatment of fuel, etc. The type of particle is very important for describing the radiative properties; in particular, the particle size, shape, and constituent species are needed. How these parameters come into play in describing the radiative properties of particles is presented in the following sections in this chapter.

## 4.2 Introduction to absorption and scattering by particles

Absorption and scattering by particles deal with the interaction of an electromagnetic wave and a small obstacle. When a wave interacts with a particle four different things can occur that are relevant for thermal radiation and are schematically shown in figure 4.1. If the wave falls directly upon the particle then it can be reflected, absorbed, or refracted. If the wave is not absorbed when passing into the particle it can go through a number of internal reflections and leave the particle in a new direction; this is called refraction. When a wave passes close to the surface of the particle its path can be bent, a phenomenon called diffraction. The scattering modes, reflection, refraction and diffraction, can be elastic or inelastic. Elastic scattering means that the scattering changes the wavelength. Only a very small portion of incoming waves go through this process. The change of wavelength by scattering is known as the Raman effect and is not relevant for thermal radiation.

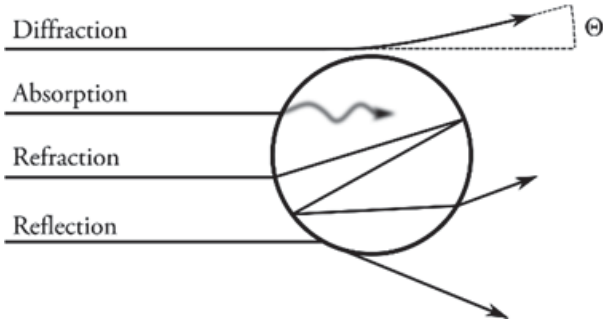


Figure 4.1. Interactions between electromagnetic waves and a spherical particle.

To determine how thermal radiation interacts with particles three parameters are commonly used. The first parameter is the complex index of refraction, $m$, of the particle, as in equation 4.1. The complex index of refraction contains the index of refraction, $n$, and the absorptive index, $k$. The index of refraction is dependent on the material of the particle but also on the wavelength. The absorptive index is also more or less dependent on the particle temperature [59]. The second parameter is the size parameter, $x$, which connects the size of the particle to the wavelength of the thermal radiation, given by equation 4.2. The last parameter is the ratio of clearance, distance between particles to wavelength, as in equation 4.3. The theory on the interaction between an electromagnetic wave starts from the interaction with a single particle. If this theory is to be applied directly to a cluster of many particles the interaction with one particle should not be affected by the presence of surrounding particles. The scattering is then said to be independent. In this case $c/\lambda \gg 1$, which is the case with most combustion applications.

$$m_\lambda = n_\lambda - ik_\lambda \tag{4.1}$$

$$x = \pi D/\lambda \tag{4.2}$$

$$c/\lambda \tag{4.3}$$

Different solution methods for the particle properties can be found in different regimes, depending on the size parameter. For the smallest size parameters, $x \ll 1$, Rayleigh scattering can be applied. For the largest particles, $x \gg 1$, geometric optics are applied. Mie-theory applies from the smallest size parameters up to sizes where geometric optics begin to be applicable. Both Mie- and Rayleigh theory concerns the scattering and absorption from single spheres. Most of the particles in combustion devices are not spherical. But when clouds of particles are considered the angular distribution of surface elements is the same for irregular and spherical particles because of their random orientation inside the cloud [60]. Methods for long infinite cylinders and the Rayleigh-Debye-Gans method for particular fractal aggregates can be used to describe non-spherical particles. Methods for applying Mie-theory to an equivalent spherical particle also exist. In this thesis all particles are assumed to be spherical.

## 4.3 Mie theory

Mie-theory is based on the theory of electromagnetism, applying Maxwell's equations to a wave traveling through a medium incident upon a sphere. It is based on the work of Gustav Mie at the beginning of the twentieth century. The advanced Mie-theory has been treated in later work by such as van der Hulst [60] and Bohren and Huffman [59]. The important parameters for thermal radiation derived from their work will be presented here. The ratio of scattered and absorbed radiation by a sphere to the incident radiation upon it is given by extinction cross-section, as

$$C_{ext} = C_{sca} + C_{abs}. \tag{4.4}$$

The cross section takes on the value of the area. The non-dimensional efficiency factors, Q, are often used instead of the cross-section. The efficiency factor relates the amount of scattering or extinction by a particle to the non-dimensionalised projected area of a sphere, as in equations 4.5 and 4.6, respectively. The absorption efficiency factor is found by subtracting the scattering from the extinction factor, as in equation 4.7. The Mie coefficients $a_n$ and $b_n$ are complex functions based on $x$ and a relative refractive index between the media and the particle. To describe the directional dependence of the scattering the phase function, $\Phi(\Theta)$, is used which gives the fraction of energy scattered in any direction. The direction, $\Theta$, is the angle between the incident and scattered wave, as presented in figure 4.1. The scattering phase function is presented in equation 4.8. The scattering phase function is proportional to the two complex amplitude functions, $S_1$ and $S_2$. The efficiency factors and amplitude functions herein derive from a computer code for Mie scattering by isotropic homogeneous spheres inspired by Bohren and Huffman, (Appendix A) [59]. An asymmetry factor, $g$, can be used to describe the phase

function. The asymmetry factor, equation 4.9, is the average cosine of the scattering angle. Equations 4.5-4.9 are presented as per Modest [6]. The asymmetry factor is defined from -1 to +1. g = -1 means that all radiation incident on the sphere is scattered backward, a value equal to zero means that all radiation is isotropically scattered, and a value of +1 means that all radiation is scattered in the forward direction. For a cloud of particles of equal size the absorption and scattering coefficient is given by equation 4.10, where $N$ is the number of particles per unit volume and $Q$ is the efficiency factor for either absorption or scattering. For particles of the same size the scattering phase function and asymmetry factor is the same for all particles. How to calculate the particle properties for varying particle sizes within the cloud is described in chapter 4.6.1.

$$Q_{sca} = \frac{C_{sca}}{\pi\left(\frac{D}{2}\right)^2} = \frac{2}{x^2}\sum_{n=1}^{\infty}(2n+1)(|a_n|^2 + |b_n|^2) \tag{4.5}$$

$$Q_{ext} = \frac{C_{ext}}{\pi\left(\frac{D}{2}\right)^2} = \frac{2}{x^2}\sum_{n=1}^{\infty}(2n+1)\Re(a_n + b_n) \tag{4.6}$$

$$Q_{abs} = \frac{C_{abs}}{\pi\left(\frac{D}{2}\right)^2} = Q_{ext} - Q_{sca} \tag{4.7}$$

$$\Phi(\Theta) = 2\frac{|S_1(\Theta)|^2 + |S_2(\Theta)|^2}{x^2 Q_{sca}} \tag{4.8}$$

$$g = \overline{\cos\Theta} = \frac{1}{4\pi}\int_{4\pi}\Phi(\Theta)\cos\Theta\, d\Omega \tag{4.9}$$

$$z_\lambda = \pi(D/2)^2 NQ, \quad z = \kappa \; or \; \sigma_s \tag{4.10}$$

## 4.4 Properties of small particles (Rayleigh theory)

The interaction of electromagnetic waves with small particles, x ≪ 1, was first studied by Lord Rayleigh in the late nineteenth century. In his work on scattering from small particles he concluded that the ratio of scattered to incident intensity on a cloud of particles is proportional to $1/\lambda^4$ [61]. With regard to the thermal radiative spectrum and the smallest particles in

combustion devices, this leads to negligible scattering [6]. According to Mie theory absorption is proportional to 1/λ [6]. For the smallest particles the size distribution does not affect the absorption coefficient, which can then be expressed by the particle volume fraction, $f_v$, [6], as

$$\kappa_\lambda = \frac{36\pi n_\lambda k_\lambda}{(n_\lambda^2 - k_\lambda^2 + 2)^2 + (2n_\lambda k_\lambda)^2} \cdot \frac{f_v}{\lambda} = \frac{C_0 f_v}{\lambda} \tag{4.11}$$

where $C_0$ is a coefficient dependent on the material of the particles. Soot is one of the commonly found small particles in combustion environments. How the presence of soot affects the predictive abilities of various gas property models is investigated in this work. Similar investigations have been carried out in several previous works [52, 53, 62-65].

## 4.5 Non-spectral particle properties

The simplest non-spectral representation of particle properties is a gray approximation. The usual one used for representing the particle properties in combustion environments is the Planck mean coefficient [8, 62, 66-68]. The Planck mean absorption coefficient is suitable for optically thin situations where emission is dominant [69]. Another gray approximation is the Rosseland mean coefficient which is suitable for optically thick situations [6]. It has been shown to be preferable to the Planck mean coefficient for pulverised coal combustion-like environments [70] but also to give large errors in a fixed bed combustion environment [8]. The Planck mean coefficients have been used and evaluated in combustion like environments in this thesis and will therefore be presented here. For soot the Planck mean absorption coefficient can be calculated using equation 4.12 [6]. The Planck mean coefficients can be calculated for any type of particle, as in equations 4.13 and 4.14, in a discretised form of the spectrum.

$$\kappa_P = 3.83 C_0 f_v T / C_2 \tag{4.12}$$

$$z_P = \left(\frac{\pi}{\sigma T^4}\right) \sum_{i=2}^{\infty} \frac{\left(I_{b,i-1} z_{i-1} + I_{b,i} z_i\right)}{2} (\lambda_i - \lambda_{i-1}), \qquad z = \kappa \; or \; \sigma_s \tag{4.13}$$

$$g_P = \frac{\sum_{i=2}^{\infty} \frac{\left(I_{b,i-1}\sigma_{s,i-1} g_{i-1} + I_{b,i}\sigma_{s,i} g_i\right)}{2} (\lambda_i - \lambda_{i-1})}{\sigma_{sP}}. \tag{4.14}$$

## 4.6 Applied modelling approaches

Particle properties have been applied on a spectral, global, and gray basis in this thesis. This section is divided into two main sub-sections which describe how the particle properties have

been applied, one for the spectral particle properties and a second one for the particle properties on both a global and a gray basis.

### 4.6.1 Spectral particle properties

Spectral particle properties were used in papers II, III, V and VI. The spectral particle properties were applied for soot in paper VI where the predictive ability of the non-correlated SNB model was evaluated. The predictive ability of radiative transfer by the non-correlated SNB approach is questionable, as mentioned in chapter 3.5.2. The presence of soot in a combustion device can lessen the importance of the gas property model as a large part of the emission and absorption comes from particles [71]. The model was therefore investigated together with soot in a number of combustion-like cases. Soot transmissivity for a homogeneous path with a distance *s* can be calculated as [72],

$$\bar{\tau}_{\Delta\eta,soot} = \exp(-C_0\bar{\eta}f_v s) \tag{4.15}$$

where the coefficient $C_0$ was set to be 5.0 in the investigated cases in paper VI. The soot transmissivity was used for the correlated SNB, the non-correlated SNB and for the GNB. For combined gas and soot transmissivity, the total transmissivity for a path was given by the product of the two. Soot was also the particle of interest in the work where radiative heat transfer was investigated in a grate fired test furnace, shown in paper V. Unlike the investigations in paper VI the properties of soot were found by using the Mie-theory. A particle mass-size distribution, presented in figure 4.2, and the refractive indexes of Chang and Charalampopoulos [73] was used to determine the absorption coefficient for the soot. The mass-size distribution for the soot, was measured in the hot flame zone in the grate fired test furnace, paper IV. To determine the spectral absorption coefficient for a particle mass-size distribution one can divide the particle sizes into a number of fractions and then sum up the contribution from these different fractions, as in equation 4.16 [74]. In papers II and III properties of fly-ash, char and unburned fuel are also considered. For these types of particles scattering can also be relevant. The scattering coefficient and the asymmetry factor are calculated by using equations 4.17 and 4.18, respectively [74]. Relevant mass-size distributions and complex index of refraction are used for the two particle types, see paper II and III. In equations 4.16-18 $\Delta m_i$ is the mass load of particles in a part of the mass-size distribution where $\bar{D}_i$ is the average particle diameter. The particle density, $\rho_{\text{part}}$, is assumed to be 1 g/cm$^3$ for all particles.

$$\kappa_\lambda = \frac{3}{2\rho_{part}} \sum_i \frac{\Delta m_i Q_{sca,\bar{D}_i,\lambda}}{\bar{D}_i} \tag{4.16}$$

$$\sigma_{s\lambda} = \frac{3}{2\rho_{part}} \sum_i \frac{\Delta m_i Q_{sca,\bar{D}_i,\lambda}}{\bar{D}_i} \tag{4.17}$$

$$g_\lambda = \frac{\sum_i \frac{\Delta m_i Q_{sca,\bar{D}_i,\lambda} g_{\bar{D}_i,\lambda}}{\bar{D}_i}}{\sigma_{s\lambda}} \tag{4.18}$$

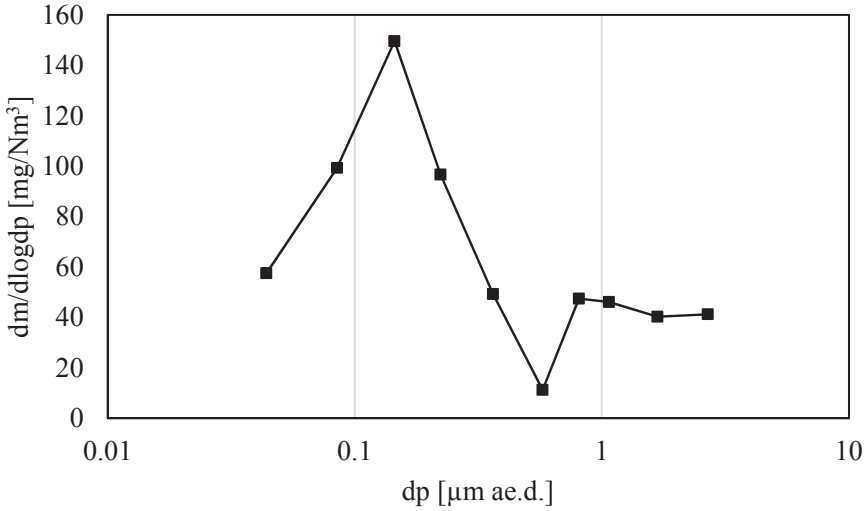


Figure 4.2. Particle mass size distribution in a grate fired test furnace for a dry gas at 10 % $CO_2$, paper IV.

As regards particles considered in this work, where scattering was relevant, most of the radiation was scattered in the forward direction. The approximate scattering phase function of Henyey-Greenstein was used, as presented in equation 4.19 [6]. The Henyey-Greenstein phase function has been shown to give good predictions for the radiative heat flux in a highly forward scattering medium by Mengüç and Viskanta [75]. To conserve the energy for the anisotropic scattering the Henyey-Greenstein phase function is normalised, as in equation 4.20, where $w_n$ is the directional weights (see chapter 2.4 (DOM-model weights)), *mn* is the scattering from direction *m* into direction *n*, and $N_O$ is the number of directions [76]. A zeroth order Δ-Eddington approximation can also be used for the strongly forward scattering particles [77] whereby some, $\sigma(1-g)$, are assumed to be scattered isotropically and the remainder assumed to be transmitted. The Δ-Eddington approximation was used to ensure the conservation of scattered energy in the 3-D cases in paper III.

$$\Phi_{HG,\lambda} = \frac{1 - g_\lambda^2}{[1 + g_\lambda^2 - 2g_\lambda cos\Theta]^{3/2}} \tag{4.19}$$

$$\frac{1}{4\pi}\sum_{n=1}^{N_o} \Phi_{HG,\lambda,mn} w_n = 1, \qquad m = 1,2,\dots,N_o. \tag{4.20}$$

In paper II and III spectral particle properties were used together with the spectral absorption coefficient for gases found by LBL calculations. The spectral coefficients of particles does not vary as erratically as the absorption coefficient of the gases does over the thermal radiative spectrum. Therefore, a larger resolution was selected for the particle properties over the spectra. For most particles the index of refraction was defined between 0.2-12 μm [68, 74]. The particle coefficients were produced in this range and divided into a thousand spectral intervals.

The spectral particle properties using Mie-theory and Rayleigh-theory have been applied in several studies investigating radiative heat transfer in combustion environments [66-68, 74, 78]. In the work carried out by Butler and Webb [67] a modelled wall heat flux was compared with a measured one in a laboratory-scale pulverised coal-fired test furnace. They concluded that for correct predictions of the wall heat flux an accurate knowledge of the char and fly-ash mass-size distribution was important. Klason et al. [66] investigated the heat flux to boundaries in a grate fired furnace by using a particle mass-size distribution taken from the measurement downstream of the furnace, from the electrostatic filters. As accurate mass-size distributions are important the effect of realistic in-furnace particle mass-size distributions was investigated in paper II. Planck mean coefficients were used for the particle properties in paper II and also in the studies [66-68]. The accuracy of spectrally averaged properties, such as the Planck mean coefficient, might not be very high, however. Large errors in heat flux and radiative source term predictions can occur. The Planck mean coefficients, specifically for fly-ash, were therefore investigated in paper III. Planck mean coefficients are elaborated in section 4.6.2.

### 4.6.2 Global and gray particle properties

The gray or spectrally averaged properties that were investigated and applied were Planck mean coefficients. Those used in paper II, III, V were temperature dependent and calculated from the spectral properties, as in equations 4.13 and 4.14. In paper II and III the Planck mean absorption coefficient, scattering coefficient and asymmetry factor were used and presented for char and fly ash. In paper V the Planck mean absorption coefficient for soot was presented and applied. The Planck mean coefficient should be used with great care, being useful for considering emission and only radiative transfer in some special cases [69]. The spectral absorption coefficient of ash particles, figure 4.3, are more non-gray than other particles. Use of Planck mean coefficients for fly-ash were therefore investigated in paper III for combustion-like environments. Implementation of the particle absorption coefficient in a global model was also investigated.

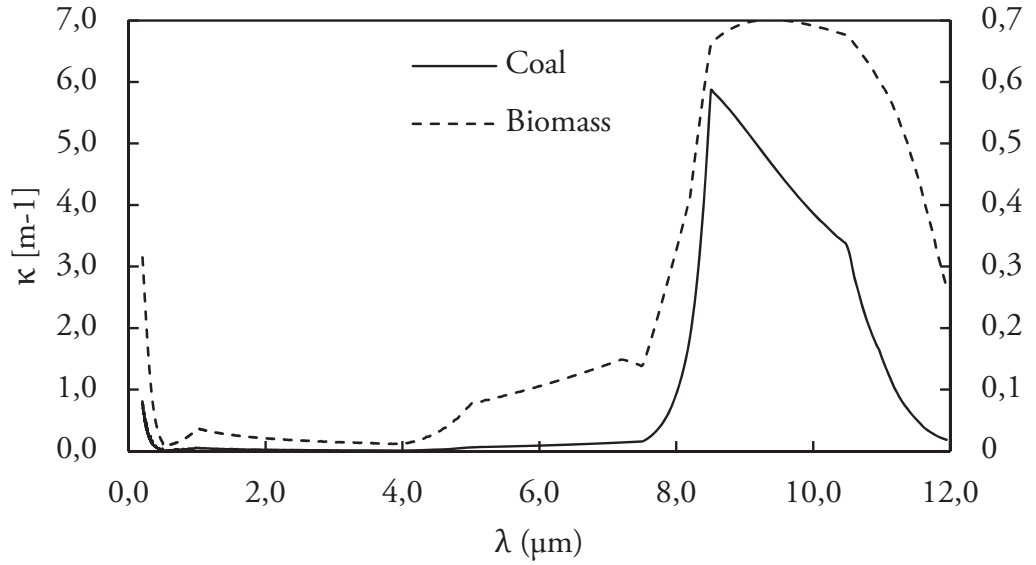


Figure 4.3. Spectral absorption coefficient of ash particles from coal (left axis) and biomass (right axis), based on paper III.

The particle properties can be implemented together with the global models for the radiative property of gases [42, 65, 79]. By combining the particle absorption coefficient with a global model one can better account for its non-grayness, compared to a gray approach. Soot particles have been implemented together with the WSGG model in previous works introducing a number of extra gray gases [54, 80, 81]. The introduction of extra gray gases doubles the computational work in these studies. The absorption coefficient of ash particles were instead incorporated to produce new WSGG parameters for a specific particle load and mole ratio for $H_2O$ and $CO_2$ in paper III. For varying particle load the same procedure adopted for varying $H_2O$ to $CO_2$ ratios was used [45, 46]. The blackbody weight coefficients and the gray band absorption coefficients were correlated by a third order polynomial fit, as in equations 4.21 and 4.22, respectively. The correlation coefficients were created for a particle load that varied between 0.1-2 times a selected base load of ash particles. More information on the procedure and the correlation coefficients can be found in paper III. In paper VI both a Planck mean coefficient and a number of extra gray gases were used to describe the soot absorption together with the WSGG model.

$$c_{i,j} = C1_{i,j} + C2_{i,j}load + C3_{i,j}load^2 + C4_{i,j}load^3, \tag{4.21}$$

$$\kappa_i = K1_i + K2_i load + K3_i load^2 + K4_i load^3. \tag{4.22}$$

# 5 Thermal radiation in grate fired furnaces

Thermal radiation in grate fired furnaces was studied in the freeboard of the furnace. This chapter will start by giving a short introduction to grate fired technology followed by the parameters that affect thermal radiation in grate fired furnaces, paper II. The second part deals with measurements, paper IV, and modelling of a 400 kW grate fired furnace, paper V.

## 5.1 Introduction to the grate fired furnace

The grate fired furnace referred to in this work is primarily a cross-fed fixed-bed furnace. Solid fuel is transferred onto a grate in the bottom of the furnace. The grate transfers the fuel further down the grate by vibrating it or by other techniques. Figure 5.1 shows a cross-section of a grate fired furnace combusting biomass. Air is supplied to the fuel, as primary air, through the grate and the rest of the air is supplied in the freeboard.

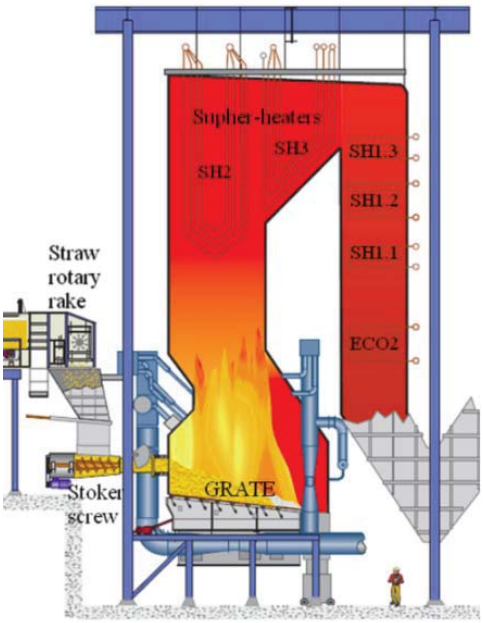


Figure 5.1. Straw-fired vibrating-grate boiler [82].

As the fuel travels along the grate it goes through the processes of drying, pyrolysis, gasification and combustion. During the drying and devolatilisation, a large part of the fuel mass is converted and transferred up into the freeboard. Left on the grate after the devolatilisation are char and bottom ash. Heterogeneous reaction between air and char completes the combustion on the grate. Both gases and particles are released into the freeboard. The suspension of particles into the freeboard increases with an increased portion of small particles in the fuel [58]. The

type of grate cooling also affects the suspension of particles. Larger amounts of particle are entrained when the grate is air-cooled rather than water-cooled [82].

The grate fired furnace technology is very fuel flexible, as it is able to combust a large variety of solid fuels with moisture content up to 60 percent. The technology is well described by Yin et al. [82], with a focus on biomass combustion. Because the technology is very fuel flexible it is also frequently used for waste incineration; in fact it is the chief combustion technology for waste incineration in Europe [83].

## 5.2 Parameters affecting thermal radiation

Thermal radiation in the grate fired furnace originates from the boundaries, the gases, and the particles. In the bottom of the furnace the walls are often covered with refractory lining. The hot flames above the bed transfer radiative heat to the refractory parts and the bed. The refractory is very hot and helps to heat up and ignite the fuel on the bed. Higher up the furnace the net radiative heat transfer goes from the hot flue gases to the colder water-membrane walls. After the first pass of the grate fired furnace the gases cool down and convection starts to dominate the heat transfer.

The parameters affecting thermal radiation which need to be determined are the properties of the participating media in the flue gases and the emissivity of the boundaries. The flue gases contain a large number of different gaseous species. As regards thermal radiation $H_2O$ and $CO_2$ are the dominant species. Other species such as CO and $CH_4$ also absorb and emit thermal radiation in the grate fired furnace but on a much lower level than $H_2O$ and $CO_2$. The particles in the flue gases can be unburned fuel, char, ash, and soot. All particles absorb and emit thermal radiation and some of them also scatter thermal radiation. The emissivity of the boundaries depends on the material on the surface and its temperature.

Thermal radiation has been studied previously in grate fired furnaces. The $P_1$-approximation was compared with the optically thin model in the prediction of the temperature field in a 55 MWe grate fired furnace by Nilsson et al. [8]. The effect on thermal radiation of fly ash in a fixed-bed biomass furnace was investigated by Bahador and Sundén [84]. The effect on the boundary heat flux and the temperature field in a 50 MW (thermal input) grate fired furnace by different radiative transport models and different gas property models together with ash and char particles was investigated by Klason et al. [66]. The investigations of thermal radiation in grate fired furnaces showed, among other things, that thermal radiation from particles is important in the grate fired furnace. The studies used particle data taken down-stream of the furnace. A study by Brunner et al. [85] on ash particles in a 20 MW grate fired furnace revealed that the particle data change significantly inside the furnace and down-stream of the furnace. Thermal radiation was therefore studied in a fixed bed furnace with realistic in-furnace ash and char particle data taken from measurements of municipal solid waste combustion and biomass

combustion in grate fired furnaces, paper II. A simple block geometry was used to represent the fixed-bed furnace. The geometry of the furnace with the temperature distribution inside is presented in figure 5.2. The geometry and temperature field were taken from the previous work of Bahador and Sundén [84]. The size of the furnace was also varied. Three furnace sizes were investigated, 2 m x 2 m x 4 m, 5 m x 5 m x 10 m, and 10 m x 10 m x 20 m. The parametric study also investigated the effect of varying emissivity of the wall and bed as there is no consensus in the literature on the different boundary emissivities. A literature study on relevant wall emissivities cited a figure of 0.5 to 1 in furnaces, paper II. Wall et al. [86] recommends that the wall emissivity should be taken from the absorptivity, which is governed by the temperature of the source of thermal radiation. Both emissivity and absorptivity decrease with increasing temperature for most combustion residues [86]. These residues are often found on the walls inside the furnace. . The difference in temperature between the source and wall can lead to large differences in representative values of wall emissivity. Total spectral values for emissivity were used in in paper II. They were shown by Bhattacharya [87] to give predictions comparable to spectral emissivities.

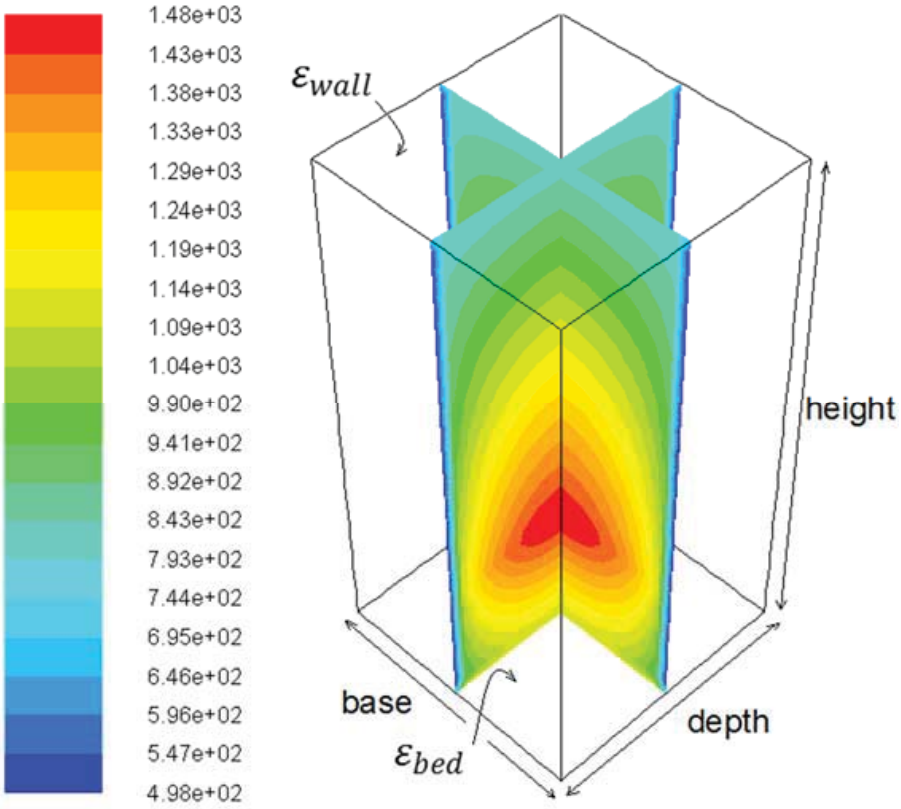


Figure 5.2. The geometry of the furnace and the temperature distribution in Kelvin, used in paper III.

## 5.3 The 400 kW grate fired test furnace

In a combustion device one can directly measure the thermal radiation which reaches a point. One can also indirectly determine the thermal radiation reaching a point by implementing measured temperatures of the flue gases, boundary temperatures, and participating media into a computational framework. The combination of these two approaches paves the way for deeper analysis of the radiative transport in a specific combustion device.

Measurements are carried out on a 400 kW grate fired test furnace combusting biomass. Being a test furnace it was designed with many access points on both the flue gas side and the water side. The large number of access points offered the opportunity to use the combined approach of direct and indirect determination of incident wall radiative flux. The measured parameters of interest were temperature of the flue gases, temperature of the boundaries, gas species mole fractions, and the particles in the flue gases. By using a combined approach one can evaluate what is contributing to the wall radiative heat flux. This chapter presents the grate fired test furnace and the measurements. It also presents how the measured parameters relevant for describing thermal radiative transport can be used and implemented in a computational framework, i.e., the indirect approach.

### 5.3.1 Description of the test furnace

The test furnace has a nominal thermal load of approximately 400 kW. It is a 5 bar hot water boiler that has a water cooled vibrating grate. Figure 5.3 shows the right side of the furnace up to the wall that separates the second and third pass. The interior height from the grate to the top is 3.5 metres and its interior width is constant at 1.05 metres. The depth varies from the bed to the top. Cartesian coordinates are given in figure 5.3 for a number of positions. The fuel used during the measurements was regular wood pellets. Information on the fuel can be found in paper IV. The fuel is transferred onto the grate by two screw feeders. During the measurement campaign, the furnace ran at approximately 400 kW, burning approximately 100 kg of fuel per hour. The primary air, which is the main air supply, is supplied in three sections through the grate, marked P1-P3 in figure 5.3. Secondary air is supplied in the freeboard from both the back and front, marked SB and SF, respectively, in figure 5.3. The furnace walls can be divided into three sections from the bed up to the top of the furnace. In the bottom of the furnace the water-membrane walls are covered with high-density refractory; above this they are covered with low density ceramic wool and higher up the water membrane walls are bare. More information on the furnace and conditions during the measurement can be found in paper IV.

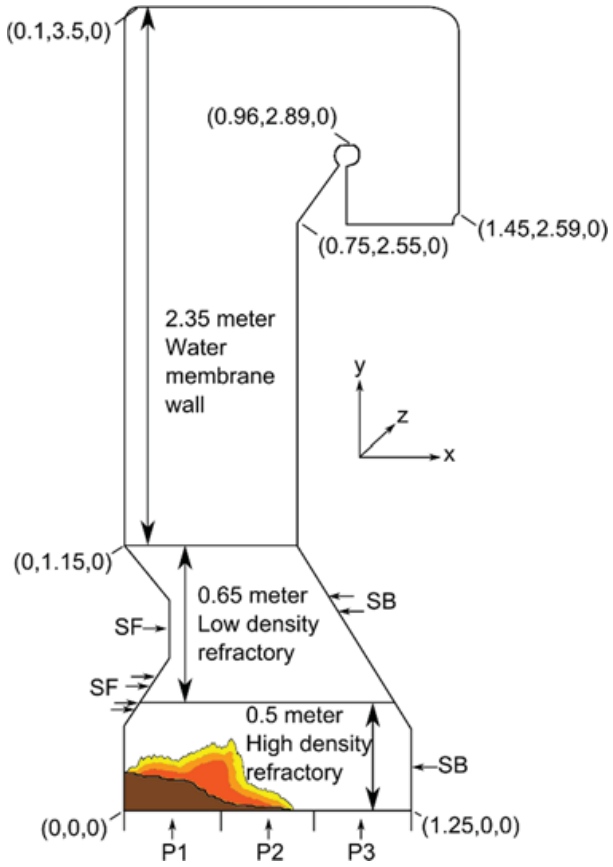


Figure 5.3. Geometry of the right side of the grate fired furnace. Presenting interior wall material at different heights, Cartesian coordinates in metres, and air supply. P stands for primary air and SF and SB stand for secondary front and back air supply, respectively, as in paper IV.

### 5.3.2 Measurements

Thermal radiation can be investigated directly by measuring the thermal radiation reaching different points of the furnace or by measuring relevant parameters for further analysis. Thermal radiation has not been measured in a grate fired furnace previously. Previous measurement studies on grate fired furnaces do not supply enough information to give a good description of the radiative transfer inside the furnace.

Thermal radiation has been measured in other combustion devices burning solid fuels or gases [67, 78, 88-92]. The measurement work was inspired by the work carried out by Butler et al. [67] on a laboratory-scale pulverised coal reactor. They also focused on the total radiative heat flux reaching the walls and therefore used a wide-angle radiometer. Most of the other studies have used a narrow angle-radiometer often combined with a cold background target.

The heat flux was measured by a wide-angle semi-ellipsoidal radiometer of the type Gunners meter [93]. Measurements were mainly carried out through the access ports on the sides of the

furnace but also on the back wall on the furnace. Almost all measurements were carried out through the sides of the furnace as most access ports were placed there. Temperature measurements were carried out on all boundaries and on the flue gases. Thermocouples and an IR-thermometer were used for measuring the temperature of the boundaries. A suction pyrometer was used for the flue gases. The temperatures of the boundaries and the flue gases had to be measured in many spatial locations to capture the temperature changes in different parts of the furnace. Measurements of the species mole fractions and the particle mass-size distribution were also carried out at a number of positions to obtain correct representation of the parameters that affect wall irradiation. The measurement procedure, devices, and errors are presented in paper IV together with the full set of measurement results.

### 5.3.3 Analysis of wall radiative heat flux

Incident radiative heat flux can be found indirectly by using measured parameters relevant to thermal radiation inside the furnace. The incident wall radiative heat flux, or wall irradiation, is found by creating a model of the furnace and implementing the measured parameters and solving the radiative transport equation. This was the method that Butler et al. [67] used for a pilot-scale pulverised coal reactor. A model for the grate-fired test furnace was set up in the commercial software ANSYS FLUENT 14.0. A temperature field was created from the discrete measurement points for both the interior and the boundaries of the furnace, as described in paper V.

The radiative transfer equation was solved for the temperature field with the measured participating media, gases and particles to find the wall incident heat flux. The relevant radiating gases, $CO_2$ and $H_2O$, were measured at close to 0.1 mole fraction in the major part of the furnace. The mole fractions of 0.1 was used in the model for the whole furnace. Particles were only measured successfully at one point in the furnace. This particle mass-size distribution was assumed be present throughout the whole furnace. As described in paper V the particles were assumed to be soot. When all the parameters are defined the solution of the radiative transport is all that remains. The accuracy of the solution depends on the radiative transport model and the radiative property models for particles and gases. As regards radiative transport model the softwares DO-method was used with a high directional and spatial discretisation to secure good accuracy. The property model for the gases in the commercial software is a gray WSGG based model, described in chapter 3.5.3. This type of model is known to give poor prediction for radiative heat transfer, particularly the source term [62, 94, 95]. A non-gray WSGG model, described in chapter 3.5.3, was therefore compared with the gray-WSGG model and a benchmarking model in plane-parallel combustion-like environments, paper V. Only the absorption coefficient was considered for the particles as they were assumed to be soot. The absorption coefficient of the particles was calculated by using Mie theory with the measured particle mass-size distribution, presented in figure 4.2, and the complex refractive index of soot

from Chang and Charalampopoulos [73] (see chapter 4.6.1 for the method of acquiring the particle properties). A Planck mean absorption coefficient, equation 4.16, was used for the gray soot absorption coefficient.

# 6 Results and discussion

The results from the investigations of thermal radiation in combustion environments are presented and discussed in this section. The chapter is divided into three main sections. The first sections are purely modelling sections. Section 6.1 concerns the 1-D cases, which are mainly plane-parallel cases, described in papers III, V and VI, but also cases along a single radiation path, as in paper I. Section 6.2 concerns 3-D furnace-like combustion environments which were investigated in papers II and III. The last section, section 6.3, presents the measured and modelled results relevant for the grate fired test furnace, described in papers IV and V.

## 6.1 1-D cases

### 6.1.1 High CO concentration environments

When thermal radiation from gases is considered in combustion environments the main radiating species of $H_2O$ and $CO_2$ are often the only relevant species. Other species such as CO and $CH_4$ are found in much smaller volume fractions and are often neglected. There are combustion environments where CO concentrations are large, such as those in gasifiers. In this work the FASTNB model [50] was extended and validated for CO. The FASTNB model is a Goody SNB model, described in chapter 3.5.2, which was used to investigate CO contribution to the radiation paths that can be found in a gasifier, paper I. Relevant data were taken from a Texaco high-pressure entrainment gasifier [96]. The investigation showed that even though the CO volume fraction is above 50 percent the contribution of CO to the total directional heat flux is minimal. The reason for this is that the relatively small volume fractions of $CO_2$ and $H_2O$ along the path still dominate the emission of radiation. This is illustrated by figure 6.1 where the spectral emissivity for $H_2O$, $CO_2$ and CO is presented for a 24 atm., 1.704 meters and 1427 K homogeneous radiation path (taken from the conditions inside the gasifier). The fundamental bands of $CO_2$ at 4.3 μm and $H_2O$ at 6.3 μm are broadened and overlap the fundamental band of CO at 4.7 μm. The relative blackbody radiation is also small where the fundamental band of CO is found. This can be seen by the smooth black curve in figure 6.1 which presents the relative blackbody radiance over the spectrum for the temperature 1427 K. The same radiation path was also investigated for lower pressures down to atmospheric pressure. At lower pressure the high CO volume fraction can make a significant contribution to the total directional radiative flux. This study only considered a single radiation path. Given the total thermal radiation reaching a point in the gasifier it is suspected that CO contribution to wall radiative heat flux could even smaller. This is because regions in the gasifier with much higher volume fractions of $H_2O$ and $CO_2$ and higher temperature would contribute to a relatively larg part of the total radiation reaching the wall.

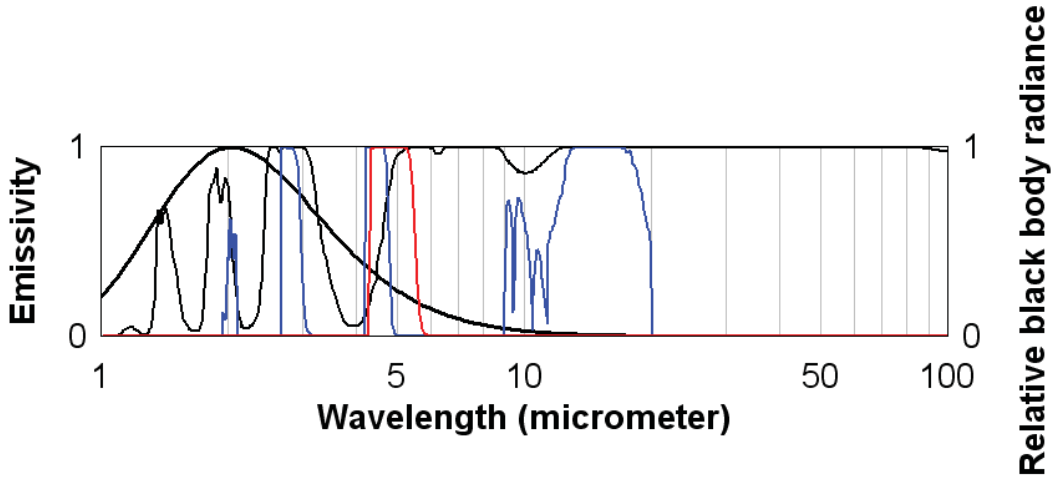


Figure 6.1. The spectral emissivity for the individual species $H_2O$ (thin black line), $CO_2$ (blue line), and CO (red line) along a homogeneous and iso-thermal radiation path. The thick black line shows the relative blackbody radiance.

### 6.1.2 The non-correlated SNB model with soot

The non-correlated statistical narrow band model was explained and presented in chapter 3.5.2. The model is introduced as a method to speed up the solution of the SNB models by dropping the spectral correlation between the transmissivity and the intensity. This method has been questioned, as described in chapter 3.5.2, but is in some cases still considered an adequate alternative to the correlated SNB, especially in combustion environments containing soot [53]. The non-correlated SNB (nc-SNB) was evaluated in a number of plane-parallel combustion-like environments with soot present, paper VI. The correlated SNB, further referred to only as SNB, and LBL calculations were used to benchmark the nc-SNB model. A gray narrow band (GNB) and WSGG models also accompanied the evaluation of the nc-SNB in the sooty environments. Two WSGG models were used, which differed in terms of how soot was introduced. One used the Planck mean absorption coefficient for soot and was referred to as WSGG-P. The other, which was named WSGG-F, used extra grey gases as per Felske and Charalampopoulos [80] to describe the soot absorption and emission The models were compared in three different types of environments. In case 1 a homogeneous environment was investigated where temperature, soot volume fraction, and distance between the planes varied. In case 2 a non-homogeneous and non-isothermal environment with two different soot loads was investigated. Case 3 was also a non-homogeneous and non-isothermal environment with a constant soot load. Unlike case 2, case 3 had a cold and a hot boundary each of which was grey. Grey boundaries were used for two reasons: to investigate the nc-SNB in a relevant environment and also to see how the SNB model performed in this type of environment. As previously mentioned in chapter 3.5.2, the correlated SNB can give erroneous results in environments with grey boundaries.

The results from case 3 are presented here. Figure 6.2 presents the source term between the hot wall, x=0 m, and cold wall, x=3 m, for the different models. Table 6.1 presents the deviation of source term and heat flux to the boundaries for all the models to the reference model, which in this case was the LBL model. The deviation of both the source term and the heat flux was rather large for the nc-SNB in comparison with the much simpler WSGG models. The reason for this is that the soot absorption and emission were not sufficiently strong at the moderate soot yield found in case 3, indicating the errors caused by the simpler treatment of the radiative transfer in the nc-SNB. It was revealed that the nc-SNB only performed better in optically thick situations, with high soot loads, and even more in optically thick and high temperature environments. The GNB model does not perform better than the nc-SNB. The much simpler WSGG model is a better option than the nc-SNB in most cases, specifically the WSGG-F, where the soot is described with extra grey gases. In case 3 the WSGG-F performs worse than the WSGG-P, see table 6.1. The reason for this is that the temperature of the media was outside the range of the soot parameters for the WSGG-F. Therefore the comparison between the WSGG-F and WSGG-P is not relevant in case 3. The emissivity was 0.8 for both boundaries in case 3. For the conditions in case 3 the SNB seems to predict the source term and heat flux very well compared with the LBL model. This indicates that the SNB model gives accurate predictions in environments with moderately reflecting boundaries and a moderate soot yield.

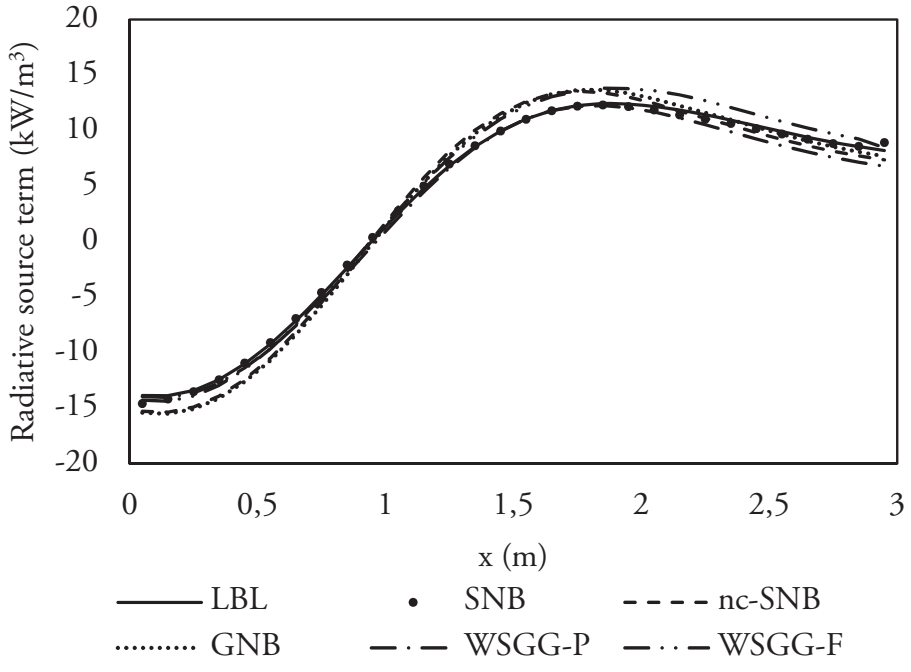


Figure 6.2. Radiative source term for case 3, paper VI.

Table 6.1. Wall heat flux from the LBL in case 3 and deviation of wall heat flux and average source term for other models, in percentage terms, paper VI.

| | $q_{w,\,x=0}$ | $q_{w,\,x=3}$ | |
|---|---|---|---|
| LBL (kW/m$^2$) | -14.7 | 25.3 | |
| | $e(q_{w,\,x=0})$ | $e(q_{w,\,x=3})$ | $e(\nabla q_{av})$ |
| SNB | 0.5 | 0.9 | 2.3 |
| nc-SNB | 14.6 | 9.8 | 10.0 |
| GNB | 12.6 | 8.3 | 9.5 |
| WSGG-P | -4.4 | 3.7 | 5.6 |
| WSGG-F* | 11.0 | 3.9 | 8.3 |

* Outside the range of the model parameters

### 6.1.3 Planck mean coefficients in combustion environments

Planck mean coefficients are often used for describing the particle properties in combustion environments. Their effect, specifically on the absorption coefficient, was commented on in chapters 4.5 and 4.6.2. In paper III the Planck mean coefficients were evaluated for fly ash in combustion-like environments, primarily in plane-parallel environments but also in a 3-D furnace-like case (which will be briefly covered in chapter 6.2). Fly-ash is interesting to evaluate as this type of particle possesses more non-gray characteristics over the spectrum (figure 4.3) compared with other particles, such as soot. The evaluation of the Planck mean coefficients in the plane-parallel environment was divided into four different cases with a constant volume fraction of $H_2O$ and $CO_2$. Two particle mass-size distributions were used in each evaluation to describe the particle properties, one that represented particles that can be found in coal-fired furnaces [87] and one for particles found in biomass combustion taken from measurements in a grate fired furnace [58]. More information on data and on the particles selected can be found in paper III. In a homogeneous case, case 1, three different path-lengths and temperatures were used between cold black walls, giving rise to 18 sub-cases with the two fly-ash types, coal and biomass. In case 2 a sinusoidal temperature profile was applied with the highest temperature in the centre. In this case, the effects of different wall emissivities were also investigated. Case 3 also applied a sinusoidal temperature profile but with a cold centre and warmer walls. Cases 1 to 3 used the same particle load over the computational domain. In a last case, case 4, a varying particle load was introduced with a load increasing from 10 percent at the wall to 200 percent at the centre of the domain, compared with the particle load used in cases 1 to 3. The Planck mean coefficients were used together with the WSGG model and compared with a reference model which used LBL calculations for the participating gases and the Mie theory to determine spectral particle properties. A new approach was also investigated and used in the comparison where the particle absorption/emission was incorporated into the WSGG parameters. To vary particle load a polynomial fit was introduced between different sets of particle loads, see chapter

4.6.2. The wall heat flux and the source term for the different models for case 4 are presented in figure 6.3, where the model named LBL uses spectral properties, WSGG+Planck uses the WSGG model for gases and Planck mean coefficients for particles, and the WSGG-particles uses the new method that was explained earlier and Planck coefficients for the scattering properties.

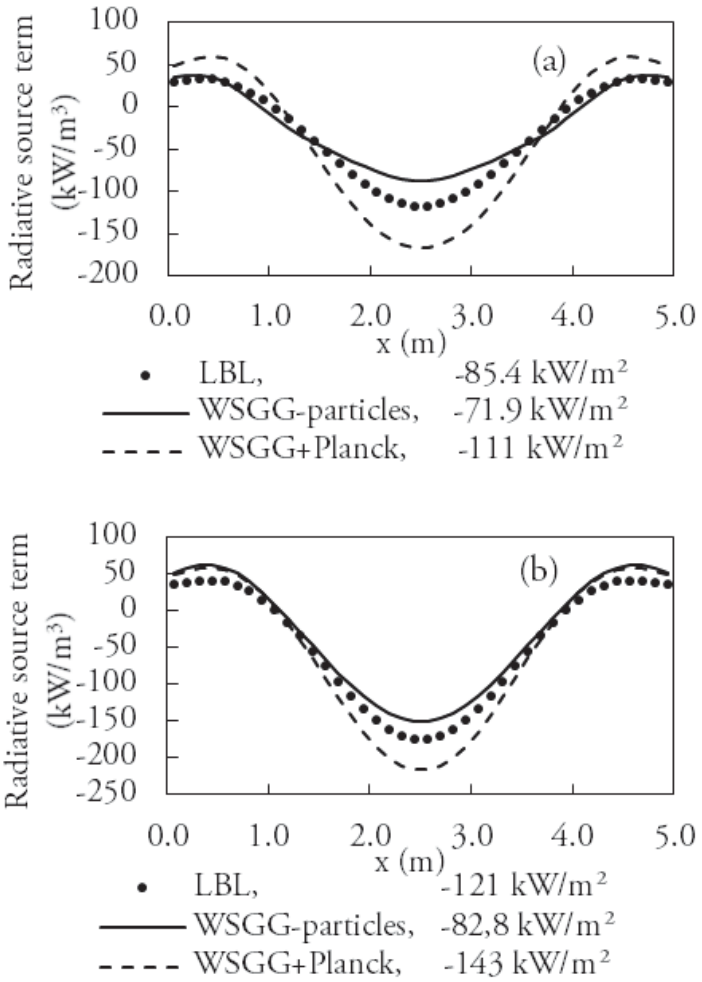


Figure 6.3. Radiative heat source and heat flux for the, LBL, WSGG-particles and WSGG+Planck in case 4 for (a) Coal, (b) Biomass.

Several cases were investigated to evaluate the accuracy of the Planck mean coefficient in relation to particle properties. For the homogeneous cases large errors could be found in prediction of both the source term and the heat flux. The largest errors for the source term were found at low temperatures and long path lengths for fly-ash from coal. An average source term deviated as much as 62 percent in such cases. The maximum error for the heat flux to the wall was 38 percent over-prediction by the WSGG+Planck. The larger errors found at long path lengths were expected as the media become optically thick in these conditions. The Planck mean coefficient is suitable for optically thin situations as it is an emission-based model. The WSGG-particles had in most homogeneous sub-cases errors that were several times smaller than the

WSGG+Planck for both the heat flux and source term. The WSGG+Planck gave large errors all through the investigated cases 1 to 4, especially for the source term. The source term predictions were better for the WSGG-particles in all cases. The heat flux predictions were somewhat higher in some cases between the two WSGG models with a maximum deviation in case 4, see figure 6.3.

### 6.1.4 Gray and non-gray WSGG models with soot

The non-gray WSGG model, often simply referred to as the WSGG model, is evaluated with soot in paper VI. The model was also applied with other combustion particles in papers II and III. The evaluated environments were either homogeneous and isothermal environments with cold walls or non-isothermal environments with rather large temperature gradients between the wall and the domain centre. As regards environments with smaller temperature gradients and with particles present the simpler gray-WSGG may be adequate to describe the absorption coefficient of the gases, described in chapter 3.5.3. Such environments exist in the grate fired furnace, specifically in the lower part of the furnace where the walls are covered by refractory. As part of paper V a grate fired test furnace is modelled in the commercial software ANSYS FLUENT 14.0, see chapter 6.2. This software uses a gray-WSGG model for $H_2O$ and $CO_2$. In paper V the gray-WSGG model, based on the WSGG parameters of Smith [97], applied in the commercial software, is compared with a non-gray WSGG model and a reference model, which used LBL calculations for the spectral absorption coefficient of the gases. The models were compared in four different plane parallel cases, with and without particles, and at two distances, 1 m. and 10 m. A rather flat temperature distribution was used across the geometry, resembling conditions in the lower part of the furnace; see paper V for more details about cases and setup. Particles properties were calculated from the measured mass-size distribution, figure 4.2, in the grate fired furnace. The particles were assumed to be soot. The spectral absorption coefficient for the soot particles was calculated with Mie-theory and the relevant particle data, as in equation 4.16. The Planck mean absorption coefficient was used for the soot particles together with the WSGG models, calculated by equation 4.13 at different temperatures. Figure 6.4 presents the source term for two cases and table 6.2 presents for all four cases the wall irradiation for the reference model and errors for the wall irradiation and source term from the non-gray WSGG and the gray WSGG model. The prediction of wall irradiation did not differ very much for the cases with soot, which was most relevant for the upcoming test furnace modelling. The source term predictions were better for the non-gray WSGG model, as the gray WSGG over-predicted the negative source term. The findings for the domain based gray-WSGG model are supported by previous studies showing that wall radiative heat flux can be predicted fairly well whereas large errors are found in the prediction of the radiative source term [95, 98].

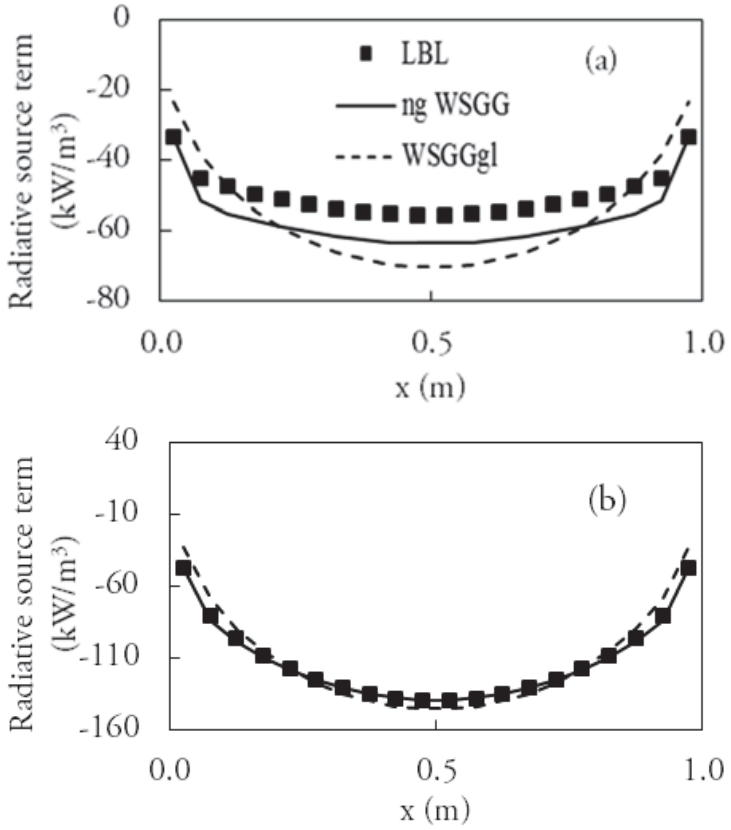


Figure 6.4. Radiative source term for plane parallel cases, a) case 1 and b) case 3, paper V.

Table 6.2. Wall irradiation, H, in kW/m², from the LBL model and relative deviation (%) for wall irradiation, centre source term and average source term for the ng WSGG and WSGGgl compared with LBL, paper V.

| | LBL | ng WSGG | | | WSGGgl | | |
|---|---|---|---|---|---|---|---|
| | H | e(H) | $e(\nabla q_{x=0.5L})$ | $e(\nabla q_{av})$ | e(H) | $e(\nabla q_{x=0.5L})$ | $e(\nabla q_{av})$ |
| Case 1 | 62.0 | -6 | -14 | 14 | -5 | -27 | 19 |
| Case 2 | 86.5 | -6 | -10 | 12 | -3 | -29 | 24 |
| Case 3 | 96.0 | 0 | 0 | 1 | 4 | -5 | 5 |
| Case 4 | 133.0 | -2 | 0 | 3 | -6 | -19 | 16 |

## 6.2 3-D cases

All 3-D cases investigated used the same geometry, with varying sizes. The geometry and an associated temperature field were presented in chapter 5.2. The investigation of the 3-D geometry is a parametric study with focus on particle radiation in grate fired furnaces, paper II, and an evaluation of the Planck mean coefficient in a 3-D geometry, paper III. In the parametric study the focus was on using realistic particle properties derived from measured or estimated in-

furnace mass-size distributions. The importance of using realistic mass-size distributions was briefly dealt with in chapter 4.6.1. The parameters affecting the thermal radiation relevant for the grate fired furnace were pointed out in chapter 5.2. Different particle mass-size distributions were considered to represent the particles in the freeboard from different fuels, mainly divided into particles from combustion of municipal solid waste (MSW) and biomass in grate fired furnaces. Different emissivities were used for the walls and the bed and different sizes of the furnace were investigated in the parametric study. In total the parametric study resulted in 60 different cases where effects on the heat flux to the bed and the walls and centreline source term were investigated. The WSGG model was used for the gases with parameters from Truelove [54]. Planck mean coefficients were used for the particle properties, as in equations 4.13 and 4.14. The spectral particle properties were found by using the Mie theory, chapter 4.3. Five different particle representations were investigated, fly ash from biomass, fly ash and char from biomass, fly ash from MSW, fly ash and char from MSW, and no particles. These representations will further be referred to as *biomass*, *biomass+char*, *MSW*, *MSW+char*, and *no particles*. The particles were assumed to be at a constant load throughout the geometry. The radiative transfer was solved with the commercial software ANSYS FLUENT 14.0 using the transfer model named DO-method. The average source term and heat flux to the wall and the bed are presented for 16 out of the 60 cases in table 6.3. Results for the bed and wall heat flux are presented for the mid-size geometry in figure 6.5 a, b; having an emissivity of 0.9 for the bed and 1.0 for the wall. The effect of scattering was also investigated by removing scattering from the two extreme particle representations *biomass* and *MSW+char*, figure 6.5 a, b.

All comparisons were made against the representation *no particles*. The source term increased with increasing size of geometry. This was expected as less radiation is transferred from the hot regions to the colder regions the larger the geometry becomes. The deviation of the source term increased with increasing furnace size for the different particle representations. The impact on the source term by *biomass* was rather small compared with *MSW*. This was also seen for the heat fluxes, see figure 6.5, and therefore this particle representation was left out of table 6.3. Changes in boundary emissivity had minor effects on the average source term. The average wall heat flux increased with increasing geometry, also as expected. When particle representations *MWS* and *MSW+char* are compared the deviation of wall heat flux does not increase as much for the *MSW* when the size of the geometry increases. The reason this lower relative increase of the wall radiative heat flux is the higher relative single-scattering albedo of the particle representation *MSW*, compared with *MSW+char*. This phenomenon of shielding the cold walls because of scattering was also shown by Marakis et al. [68]. The particle effect was most significant for the bed heat flux, where relevant effects were seen for all particle representations, especially in the large geometry. The scattering caused an increase of the heat flux to the bed, see figure 6.5 a. The reason for this was that a small part of the radiation leaving the bed was reradiated back. This scattering effect for the bed heat flux was not as significant as for the wall

heat flux, figure 6.5 b. The effect of the emissivity on the heat fluxes to the boundaries was large. Obviously the changed emissivity of a boundary had an effect on the heat flux to that boundary. Large effects on the heat flux to the bed were seen when the wall emissivity was changed. With a reflecting wall, which had an emissivity of 0.5, the heat flux to the bed increased by more than 20 percent compared with a non-reflecting wall.

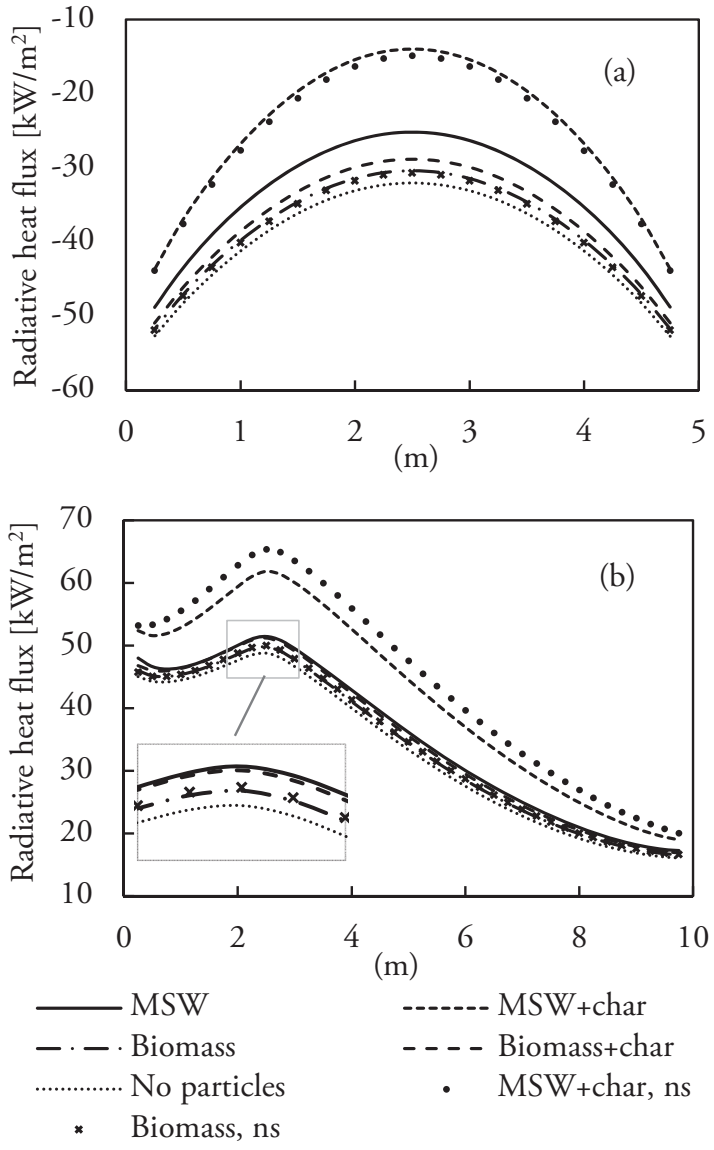


Figure 6.5. Radiative heat flux to the centreline of the bed (a) and the wall (b) for different fuel parameters. *ns* = non-scattering.

Table 6.3. The average source term along the centreline of the furnace, the average heat flux to the centreline of the wall, and the average heat flux centreline of the bed for the representation *no particles.* Percentile deviation for the particle representations *biomass+char*, *MSW*, and *MSW+char*, in that order.

| Size ($m^3$) | $\varepsilon_{wall}$ | $\varepsilon_{bed}$ | $\nabla\bar{q}$ | | | $\bar{q}_{wall}$ | | | $\bar{q}_{bed}$ | | |
|---|---|---|---|---|---|---|---|---|---|---|---|
| 2x2x4 | 0.5 | 0.7 | -47.4 kW/$m^3$ | | | 16.3 kW/$m^2$ | | | -30.0 kW/$m^2$ | | |
| | | | -6 | -16 | -43 | -4 | -5 | -20 | 4 | 8 | 24 |
| 2x2x4 | 1 | 0.9 | -51.8 kW/$m^3$ | | | 28 kW/$m^2$ | | | -47.2 kW/$m^2$ | | |
| | | | -6 | -15 | -42 | -3 | -6 | -21 | 3 | 8 | 19 |
| 10x10x20 | 0.5 | 0.7 | -14.7 kW/$m^3$ | | | 19.8 kW/$m^2$ | | | -22.6 kW/$m^2$ | | |
| | | | -14 | -47 | -84 | -10 | -7 | -28 | 18 | 23 | 59 |
| 10x10x20 | 1 | 0.9 | -16.3 kW/$m^3$ | | | 35.9 kW/$m^2$ | | | -34.9 kW/$m^2$ | | |
| | | | -13 | -39 | -75 | -8 | -7 | -29 | 13 | 23 | 55 |

The Planck mean coefficients were used for the particle radiative properties in the parametric study in paper II. An evaluation of the Planck mean coefficients in combustion environments was carried out in paper III. This study revealed that large errors are related to predictions of both the heat flux and source term when Planck mean coefficient are used for fly-ash particles, see also chapter 6.1.3. As regards the 3-D geometry, which was also investigated in paper III, the errors from using the Planck mean coefficient were estimated to be within 20 percent. The importance of the different parameters for a parametric study was investigated and not their absolute values. Therefore the investigations and results are considered to hold even though Planck mean coefficients were used to describe the radiative properties of the fly-ash particles

## 6.3 The grate fired test furnace

Modelling and measurements were carried out in a 400 kW grate fired test furnace. The measurements results are found in paper IV in full. The modelling of the furnace was carried out in paper V. Chapter 5 gives an introduction to the grate fired furnace technology, the grate fired test furnace, and the specific measurements in the furnace. Chapter 5 also presents the modelling procedure, radiative transport and property models that were used for the furnace. Like the previous cases in this chapter the solution of the radiative transfer equation was carried out for a fixed temperature field. The big difference between the previous cases and this case is that a temperature field was created from real temperature measurements of the flue gases inside the furnace for a geometry created by using dimensions of the test furnace. The temperatures of the walls and bed were also measured and implemented in the model. Figure 6.6 presents the measured temperatures close to the centre-plane, seen from the side of the furnace, together

with the interpolated temperature field at the centre of the furnace, seen from the side. In total, 41 flue gas temperatures were measured throughout the furnace with a focus in the lower part of the furnace where the highest temperature gradients are found. More information on the interpolation scheme used to create the temperature field from the discrete measurement points can be found in paper V.

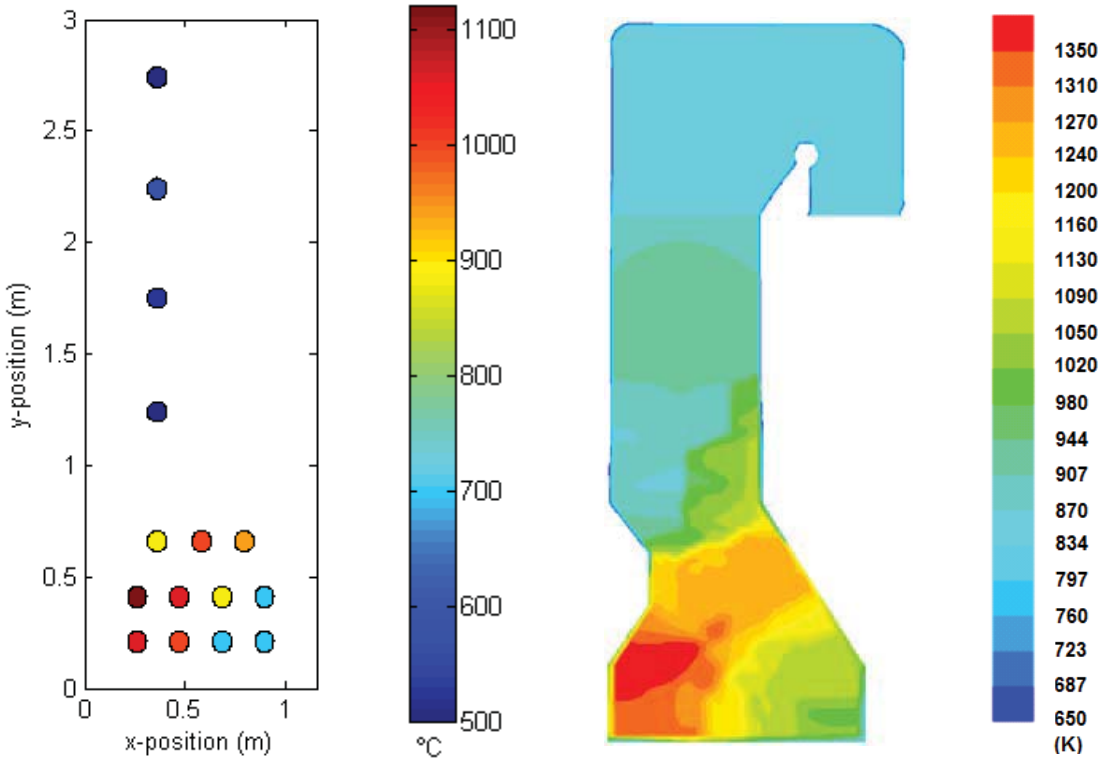


Figure 6.6. Measured temperatures of the flue gases close to the central plane seen from the side in the grate fired furnace, left figure paper IV, and the interpolated temperature field in the central plane seen from the side of the furnace, right figure paper V.

The investigation of thermal radiation in the grate fired test furnace focused on the wall irradiation. The wall irradiation was measured at several positions on the furnace. The measured and modelled wall irradiation along a vertical line on the right side of the furnace is presented in figure 6.7. The property models and the input data used for describing the participating media are presented in chapter 5.3.2 and 6.1.3. The gray WSGG model, WSGGgl, and the non-gray WSGG model, ng WSGG, predict a wall irradiation that does not differ very much. The small difference between the property models in the prediction of wall irradiation was also seen in the evaluations of the models, in chapter 6.1.3. Large under-predictions were found in the lower parts of the furnace compared with the measured wall irradiation. There are several reasons for this under-prediction. The main reason for the difference in wall irradiation was concluded to be particles that were not measured in the furnace. Particle measurement inside

the furnace is a complex endeavour. Details about the particle measurement can be found in paper IV. Large particles were missed because the instrument that was used could only measure sizes up to 10 µm. Some particles in the range of 1-10 µm were also lost inside the sampling system. From the comparison between the measured wall irradiation and the modelled wall irradiation without particles present, curve with legend ng WSGG in figure 6.7, it could be seen that the particles almost doubled the wall irradiation in the lower part of the furnace. A modelled wall irradiation without any participating media is also presented in figure 6.7. This curve reveals that in the evaluated test furnace the surrounding boundaries give a large contribution to the wall irradiation. This contribution is expected to be smaller in larger industrial-size furnaces because of the longer pressure-path lengths that exist in these furnaces.

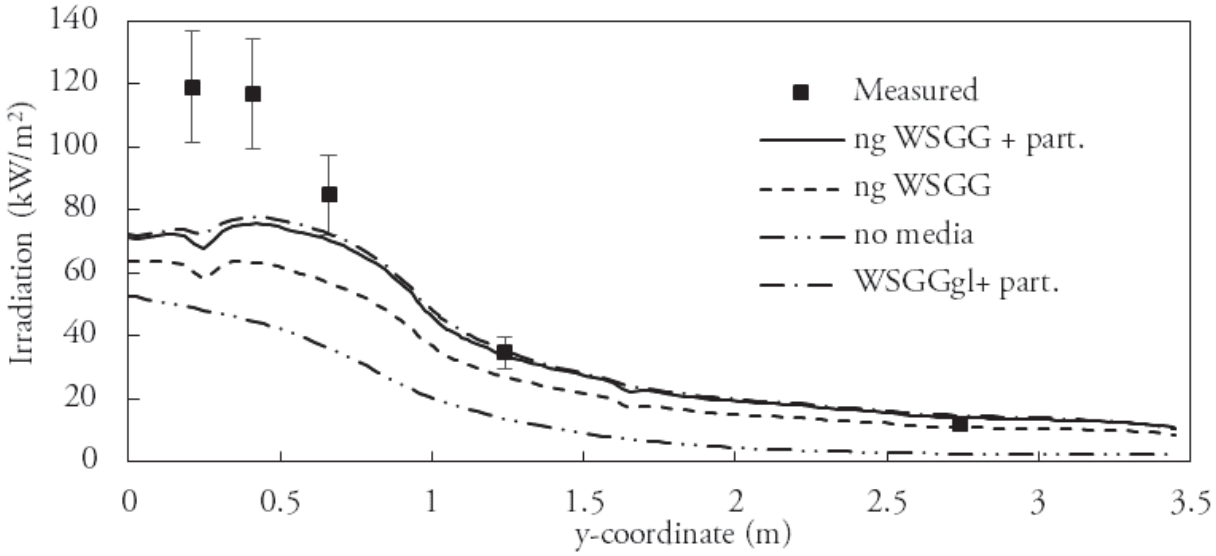


Figure 6.7. Furnace wall irradiation at the right wall from the bed to the top of the furnace along the line, (x, y, z)=(0.36, y, 0), paper V.

# 7 Conclusions and future outlook

This chapter presents the conclusions and possible future outlook in relation to each paper on which this thesis is based.

**Paper I**

A FASTNB model, a version to speed up the computation of the SNB model found in the computational code RADCAL, was extended and validated for the species CO. Investigations were carried out on CO contribution to the total directional radiative heat flux in environments containing high CO concentrations, specifically the environment found in a high pressure gasifier. Even though CO concentrations can locally reach values above 50 percent volume fraction, in such environments its contribution to the total directional heat flux is minor. The reason for this is that such environments still contain $H_2O$ and $CO_2$ which, albeit in much smaller volume fractions, still make the greatest contribution to the directional radiative heat flux.

The small contribution from CO to the total directional radiative heat flux was caused by overlapping from $CO_2$ and $H_2O$ on its fundamental vibration-rotation band. This overlap was shown to decrease with decreasing pressure, giving rise to a larger contribution from CO to the directional radiative heat flux. The impact of using only a single radiation path was discussed in chapter 6.1.1. It would be interesting to study CO contribution to the wall radiative heat flux and the radiative source term in a full-scale 3-D gasifier operating close to atmospheric pressure.

**Paper II**

A parametric study on thermal radiation in grate fired furnace-like environments was carried out. The main focus was placed on particle radiation effects; however, the impact of varying boundary emissivity and furnace size was also investigated. Compared with previous studies realistic in-furnace particle information was used for char and fly-ash particles from MSW and biomass combustion. MSW combustion produces much more particles than biomass combustion. Hence the largest effects on boundary heat fluxes and source term were seen in cases with particle from MSW combustion. Char particle load was estimated from recorded fractions of unburned fuel in fly-ash samples taken downstream in grate fired furnaces. The char particles were shown to have a significant effect on the particle radiation in the furnace. The contribution from particle radiation increased with increasing furnace size. This was expected, as larger pressure path-lengths are found in the larger geometries. The choice of an accurate

boundary emissivity was shown to be equally as important as the effects of particle radiation from MSW particle when the heat fluxes to the boundaries were considered.

Char particles were shown to make a large contribution to the particle radiation in the furnace. Being estimated from furnace downstream values the particle load inside the furnace is associated with large uncertainties. Measurement studies are needed on unburned fuel and char particles inside the furnace to get a more certain representation of the particles. Soot was not considered in the study. A later study has shown, paper V, that soot can give a large contribution to the particle radiation in the hot flame zone of the grate fired furnace. Therefore the inclusion of soot in the hot flame region would also give a better representation of particle radiation inside the grate fired furnace. A simple furnace geometry was used to represent the grate fired furnace in the parametric study. The bed had a high temperature representing the part where only char is left on the grate. The particle load was also assumed to be equally distributed throughout the furnace. The effect of changing particle load distributions and a more realistic furnace geometry would be of interest in further studies.

**Paper III**

The Planck mean coefficients have been evaluated in combustion environments with realistic particle mass-size distributions of fly-ash particles. The study reveals that using Planck mean coefficient for fly-ash particles is associated with large errors in prediction of both the radiative source term and the wall radiative heat flux. A new approach that incorporated the particle absorption coefficient into a WSGG model was evaluated. This approach showed promising results compared with the use of a Planck mean absorption coefficient in environments with constant particle load throughout the geometry. When particle load changed within the geometry large errors were seen with this approach.

In combustion environments where fly-ash exists one often also finds other particles, such as char, unburned fuel and soot. Incorporating all these particles in a WSGG model might be problematic and tedious. To account for various particle loads it might be better to represent each type of particle by a number of extra gray gases instead. This would then lead to larger computational demand as increased number of gray gases leads to extra solutions of the RTE. A study would be of interest where all types of particles individual importance are evaluated to the overall thermal radiation in a grate fired furnace. New computationally efficient and accurate alternatives to the Planck mean coefficient are needed.

**Paper IV**

This paper present a comprehensive measurements study of the parameters relevant for thermal radiation in a 400 kW grate fired test furnace. The results of the study can be divided into two parts: direct measurement of the wall irradiation and the measured parameters that can be used

to indirectly determine the wall irradiation. The measured parameters that can be used in an indirect approach are the flue gas temperature, the wall and bed temperature, gas species volume fractions, and particle mass-size distribution. In the test furnace a larger fraction of the supplied air is introduced as primary air than in a commercial grate fired furnace. This could mean more particles are entrained into the freeboard of the furnace.

The particle measurement was limited to particle sizes lower than 10 µm. Particle measurement of sizes larger than the measured sizes would therefore be of interest. More information on the particles inside the furnace would be possible to obtain by using a narrow-angle measurement device with a selectable narrow spectral range. The purpose of the study was to gain deeper knowledge into thermal radiation in grate fired furnace. To broaden the study´s field of application it would be of interest to study the impact of various fuel sizes and fuel types on the wall irradiation.

**Paper V**

The parameters measured in the grate fired test furnace for the indirect approach, paper IV, were applied to a geometry where the radiative transfer equation is solved. Two models were used for the gas properties, the gray- and non-gray WSGG model. For the purpose of predicting the wall irradiation the two models compare very well. In terms of radiative heat source prediction the non-gray WSGG model outperforms the gray-WSGG model. Comparison between the modelled wall irradiation, via the indirect approach, and the measured wall radiation reveal that a large part of wall irradiation comes from the particles, specifically in the hot flame zone of the furnace. The surrounding boundaries also make a large contribution to the wall irradiation in the modelled test furnace. The modelled wall irradiation did not match the measured wall irradiation, especially in the hot flame zone. The reason for this is assumed to be the particles that were missed during the measurement. Also, it might relate to particles having a higher temperature than the measured flue gas temperature, which is an average of gas and particle temperature.

It would be of interest to implement more particle data in continued study of a furnace where the different particle types and their temperature have been measured.

**Paper VI**

A non-correlated SNB model was compared with benchmark models and other simpler models. The non-correlated SNB is suggested in the literature to be a fast alternative to the SNB model, specifically in sooty environments. In most investigated cases the non-correlated SNB gives less accurate predictions than the simpler WSGG models, which were also included in the evaluation. Only in optically thick situations and specifically at high temperature did the non-correlated SNB perform better than the other investigated models. Because of the limited

instances where the non-correlated SNB performs better, and the fact that the model demands a much larger computational demand compared with the simpler global model, it is not recommended for use even in sooty environments. With regards to optically thick situations other radiative property models should be used than the ones investigated in this study.

# References


[1] BP, BP Statistical review of world energy consumption 2014, Brittish Petroleum, 2014

[2] Shafiee, S.,Topal, E., When will fossil fuel reserves be diminished?, Energy Policy, 37(1), pp. 181-189, 2009

[3] Viskanta, R.,Mengüç, M.P., Radiation heat transfer in combustion systems, Progress in Energy and Combustion Science, 13(2), pp. 97-160, 1987

[4] Planck, M., Ueber das Gesetz der Energieverteilung im Normalspectrum, Annalen der Physik, 309(3), pp. 553-563, 1901

[5] Wien, W., Temperatur und entropie der strahlung, Annalen der Physik, 288(5), pp. 132-165, 1894

[6] Modest, M.F., Radiative Heat Transfer Vol. 2, Burlington Academic Press, p. 822, 2003

[7] Viskanta, R., Computation of radiative transfer in combustion systems, International Journal of Numerical Methods for Heat and Fluid Flow, 18(3-4), pp. 415-442, 2008

[8] Nilsson, T., Klason, T., Bai, X.-S.,Sundén, B., Thermal radiation heat transfer and biomass combustion in a large-scale fixed bed boiler, in ASME 2003 International Mechanical Engineering Congress and Exposition. American Society of Mechanical Engineers,p. 405-413, 2003

[9] Lockwood, F.C.,Shah, N.G., A new radiation solution method for incorporation in general combustion prediction procedures, Symposium (International) on Combustion, 18(1), pp. 1405-1414, 1981

[10] Raithby, G.D.,Chui, E.H., A finite-volume method for predicting a radiant heat transfer in enclosures with participating media, Journal of Heat Transfer, 112(2), pp. 415-423, 1990

[11] Chandrasekhar, S., Radiative transfer, New York Dover Publications Inc, p. 393, 1960

[12] Fiveland, W.A., Discrete ordinate methods for radiative heat transfer in isotropically and anisotropically scattering media, Journal of Heat Transfer, 109(3), pp. 809-812, 1987

[13] Mishra, S.C., Roy, H.K.,Misra, N., Discrete ordinate method with a new and a simple quadrature scheme, Journal of Quantitative Spectroscopy and Radiative Transfer, 101(2), pp. 249-262, 2006

[14] Kim, T.K., Menart, J.A.,Lee, H.S., Nongray radiative gas analyses using the SN discrete ordinates method, Journal of Heat Transfer, 113(4), pp. 946-952, 1991

[15] Lee, H.S., Chai, J.C.,Patankar, S.V., Recent Developments in the Solution of Radiation Heat Transfer Using the Discrete Ordinates Method, International Journal of Fluid Mechanics Research, 25(4-6), pp., 1998

[16] Singh, R.,Mishra, S.C., Analysis of Radiative Heat Transfer in a Planar Participating Medium Subjected to Diffuse and/or Collimated Radiation—A Comparison of the

DTM, the DOM, and the FVM, Numerical Heat Transfer, Part A: Applications, 52(5), pp. 481-496, 2007

[17] Seung H. Kim, K.Y.H., Assessment of the finite-volume method and the discrete ordinate method for radiative heat transfer in a three-dimensional rectangular enclosure, Numerical Heat Transfer, Part B: Fundamentals, 35(1), pp. 85-112, 1999

[18] Fischer, J., Gamache, R.R., Goldman, A., Rothman, L.S.,Perrin, A., Total internal partition sums for molecular species in the 2000 edition of the HITRAN database, Journal of Quantitative Spectroscopy and Radiative Transfer, 82(1–4), pp. 401-412,

[19] Herzberg, G., Molecular spectra and molecular structure, New York van Nostrand, 1966

[20] Rothman, L.S., Rinsland, C.P., Goldman, A., Massie, S.T., Edwards, D.P., Flaud, J.M., Perrin, A., Camy-Peyret, C., Dana, V., Mandin, J.Y., Schroeder, J., McCann, A., Gamache, R.R., Wattson, R.B., Yoshino, K., Chance, K.V., Jucks, K.W., Brown, L.R., Nemtchinov, V.,Varanasi, P., The HITRAN molecular spectroscopic database and Hawks (HITRAN atmospheric workstation): 1996 edition, Journal of Quantitative Spectroscopy and Radiative Transfer, 60(5), pp. 665-710, 1998

[21] McClatchey, R.A., Benedict, W., Clough, S., Burch, D.,Calfee, R., AFCRL atmospheric absorption line parameters compilation, DTIC Document, 1973

[22] Rothman, L.S., Gordon, I.E., Babikov, Y., Barbe, A., Chris Benner, D., Bernath, P.F., Birk, M., Bizzocchi, L., Boudon, V., Brown, L.R., Campargue, A., Chance, K., Cohen, E.A., Coudert, L.H., Devi, V.M., Drouin, B.J., Fayt, A., Flaud, J.M., Gamache, R.R., Harrison, J.J., Hartmann, J.M., Hill, C., Hodges, J.T., Jacquemart, D., Jolly, A., Lamouroux, J., Le Roy, R.J., Li, G., Long, D.A., Lyulin, O.M., Mackie, C.J., Massie, S.T., Mikhailenko, S., Müller, H.S.P., Naumenko, O.V., Nikitin, A.V., Orphal, J., Perevalov, V., Perrin, A., Polovtseva, E.R., Richard, C., Smith, M.A.H., Starikova, E., Sung, K., Tashkun, S., Tennyson, J., Toon, G.C., Tyuterev, V.G.,Wagner, G., The HITRAN2012 molecular spectroscopic database, Journal of Quantitative Spectroscopy and Radiative Transfer, 130(0), pp. 4-50, 2013

[23] Rothman, L.S., Gordon, I.E., Barber, R.J., Dothe, H., Gamache, R.R., Goldman, A., Perevalov, V.I., Tashkun, S.A.,Tennyson, J., HITEMP, the high-temperature molecular spectroscopic database, Journal of Quantitative Spectroscopy and Radiative Transfer, 111(15), pp. 2139-2150, 2010

[24] Chu, H., Liu, F.,Zhou, H., Calculations of gas thermal radiation transfer in one-dimensional planar enclosure using LBL and SNB models, International Journal Heat Mass Transfer, 54(21-22), pp. 4736-4745, 2011

[25] Elsasser, W.M., Mean Absorption and Equivalent Absorption Coefficient of a Band Spectrum, Physical Review, 54(2), pp. 126-129, 1938

[26] Goody, R.M., A statistical model for water vapour absorption, Quart. J. Roy. Meteor. Soc, 78165-169, 1952

[27] Arking, A.,Grossman, K., The Influence of Line Shape and Band Structure on Temperatures in Planetary Atmospheres, Journal of the Atmospheric Sciences, 29(5), pp. 937-949, 1972

[28] Edwards, D.K.,Menard, W.A., Comparison of models for correlation of total band absorption, Applied Optics, 3(5), pp. 621-625, 1964
[29] Malkmus, W., Random Lorentz Band Model with Exponential-Tailed S-1 Line-Intensity Distribution Function, J. Opt. Soc. Am., 57(3), pp. 323-329, 1967
[30] Ludwig, C.B., Malkmus, W., Reardon, J.E.,Thomson, J.A.L., Handbook of infrared radiation from combustion gases, NASA SP-3080, Washington, D.C., 1973
[31] Grosshandler, W.L., Radiative heat transfer in nonhomogeneous gases: A simplified approach, International Journal of Heat and Mass Transfer, 23(11), pp. 1447-1459, 1980
[32] Grosshandler, W., RADCAL: A narrow band model for radiation calculations in a combustion environment, Gaithersburg, MD 20899, 1993
[33] Soufiani, A., Hartmann, J.M.,Taine, J., Validity of band-model calculations for $CO_2$ and $H_2O$ applied to radiative properties and conductive-radiative transfer, Journal of Quantitative Spectroscopy and Radiative Transfer, 33(3), pp. 243-257, 1985
[34] Soufiani, A.,Taine, J., High temperature gas radiative property parameters of statistical narrow-band model for $H_2O$, $CO_2$ and CO, and correlated-K model for $H_2O$ and $CO_2$, International Journal Heat Mass Transfer, 40(4), pp. 987-991, 1997
[35] Marakis, J.G., Application of narrow and wide band models for radiative transfer in planar media, International Journal of Heat and Mass Transfer, 44(1), pp. 131-142, 2001
[36] Young, S.J., Nonisothermal band model theory, Journal of Quantitative Spectroscopy and Radiative Transfer, 18(1), pp. 1-28, 1977
[37] Taine, J.,Soufiani, A., Gas IR Radiative Properties: From Spectroscopic Data to Approximate Models, Advances in Heat Transfer, Volume 33295-414, 1999
[38] Pierrot, L., Soufiani, A.,Taine, J., Accuracy of narrow-band and global models for radiative transfer in $H_2O$, $CO_2$, and $H_2O$-$CO_2$ mixtures at high temperature, Journal of Quantitative Spectroscopy and Radiative Transfer, 62(5), pp. 523-548, 1999
[39] Hottel, H.C.,Sarofim, A.F., Radiative heat transfer, New York McGrawHill, p. 520, 1967
[40] Denison, M.K.,Webb, B.W., Spectral line-based weighted-sum-of-gray-gases model for arbitrary RTE solvers, Journal of Heat Transfer 115(4), pp. 1004-1012, 1993
[41] Denison, M.K.,Webb, B.W., An absorption-line blackbody distribution function for efficient calculation of total gas radiative transfer, Journal of Quantitative Spectroscopy and Radiative Transfer, 50(5), pp. 499-510, 1993
[42] Modest, M.F.,Zhang, H., The Full-Spectrum Correlated-k Distribution for Thermal Radiation From Molecular Gas-Particulate Mixtures, Journal of Heat Transfer, 124(1), pp. 30-38, 2002
[43] Pierrot, L., Rivière, P., Soufiani, A.,Taine, J., A fictitious-gas-based absorption distribution function global model for radiative transfer in hot gases, Journal of Quantitative Spectroscopy and Radiative Transfer, 62(5), pp. 609-624, 1999
[44] Modest, M.F., The weighted-sum-of-gray-gases model for arbitrary solution methods in radiative transfer, ASME Journal of Heat Transfer, 113650-656, 1991

[45] Johansson, R., Leckner, B., Andersson, K.,Johnsson, F., Account for variations in the $H_2O$ to $CO_2$ molar ratio when modelling gaseous radiative heat transfer with the weighted-sum-of-grey-gases model, Combustion and Flame, 158(5), pp. 893-901, 2011

[46] Kangwanpongpan, T., França, F.H.R., Corrêa da Silva, R., Schneider, P.S.,Krautz, H.J., New correlations for the weighted-sum-of-gray-gases model in oxy-fuel conditions based on HITEMP 2010 database, International Journal of Heat and Mass Transfer, 55(25-26), pp. 7419-7433, 2012

[47] Soufiani, A.,Djavdan, E., A comparison between weighted sum of gray gases and statistical narrow-band radiation models for combustion applications, Combustion and Flame, 97(2), pp. 240-250, 1994

[48] Goutiere, V., Liu, F.,Charette, A., An assessment of real-gas modelling in 2-D enclosures, Journal of Quantitative Spectroscopy and Radiative Transfer, 64(3), pp. 299-326, 2000

[49] Liu, F., Gülder, Ö.L., Smallwood, G.J.,Ju, Y., Non-grey gas radiative transfer analyses using the statistical narrow-band model, International Journal of Heat and Mass Transfer, 41(14), pp. 2227-2236, 1998

[50] Yan, Z.,Holmstedt, G., Fast, narrow-band computer model for radiation calculations, Numerical Heat Transfer, Part B, 31(1), pp. 61-71, 1997

[51] Abu-Romia, M.M.,Tien, C.L., Measurements and correlations of infrared radiation of carbon monoxide at elevated temperatures, Journal of Quantitative Spectroscopy and Radiative Transfer, 6(2), pp. 143-167, 1966

[52] Zhang, L., Soufiani, A.,Taine, J., Spectral correlated and non-correlated radiative transfer in a finite axisymmetric system containing an absorbing and emitting real gasparticle mixture, International Journal of Heat and Mass Transfer, 31(11), pp. 2261-2272, 1988

[53] Yan, Z.H., A Fast Spectral Approximation of Narrow-band Model for Thermal Radiation Calculation, Numerical Heat Transfer, Part B, 46(2), pp. 165-178, 2004

[54] Truelove, J.S., The zone method for radiative heat transfer calculations in cylindrical geometries, Automatic Energy Authority, Harwell, 1975

[55] Lallemant, N., Sayre, A.,Weber, R., Evaluation of emissivity correlations for H2O---CO2---N2/air mixtures and coupling with solution methods of the radiative transfer equation, Progress in Energy and Combustion Science, 22(6), pp. 543-574, 1996

[56] Mansurov, Z., Soot formation in combustion processes (review), Combustion, Explosion and Shock Waves, 41(6), pp. 727-744, 2005

[57] Williams, A., Jones, J.M., Ma, L.,Pourkashanian, M., Pollutants from the combustion of solid biomass fuels, Progress in Energy and Combustion Science, 38(2), pp. 113-137, 2012

[58] Brunner, T., Aerosols and coarse fly ashes in fixed-bed biomass combustion, Ph.D. thesis, Institute of Resource Efficient and Sustainible Systems, Graz: Graz University of Technology, p. 158, 2006

[59] Bohren, C.F.,Huffman, D.R., Absorption and scattering of light by small particles, New York John Wiley & Sons, p. 544, 1998
[60] Hulst, H.C.,Van De Hulst, H., Light scattering by small particles, Courier Corporation, 1957
[61] Strutt, J.W., XV. On the light from the sky, its polarization and colour, The London, Edinburgh, and Dublin Philosophical Magazine and Journal of Science, 41(271), pp. 107-120, 1871
[62] Demarco, R., Consalvi, J.L., Fuentes, A.,Melis, S., Assessment of radiative property models in non-gray sooty media, International Journal of Thermal Sciences, 50(9), pp. 1672-1684, 2011
[63] Bressloff, N.W., The influence of soot loading on weighted sum of grey gases solutions to the radiative transfer equation across mixtures of gases and soot, International Journal of Heat and Mass Transfer, 42(18), pp. 3469-3480, 1999
[64] Wang, L., Modest, M.F., Haworth, D.C.,Turns, S.R., Modelling nongrey gas-phase and soot radiation in luminous turbulent nonpremixed jet flames, Combustion Theory and Modelling, 9(3), pp. 479-498, 2005
[65] Solovjov, V.P.,Webb, B.W., An efficient method for modeling radiative transfer in multicomponent gas mixtures with soot, Journal of Heat Transfer, 123450, 2001
[66] Klason, T., Bai, X.S., Bahador, M., Nilsson, T.K.,Sundén, B., Investigation of radiative heat transfer in fixed bed biomass furnaces, Fuel, 87(10-11), pp. 2141-2153, 2008
[67] Butler, B., Denison, M.,Webb, B., Radiation heat transfer in a laboratory-scale, pulverized coal-fired reactor, Experimental Thermal and Fluid Science, 9(1), pp. 69-79, 1994
[68] Marakis, J.G., Papapavlou, C.,Kakaras, E., A parametric study of radiative heat transfer in pulverised coal furnaces, International Journal of Heat and Mass Transfer, 43(16), pp. 2961-2971, 2000
[69] Siegel, R.,Howell, J.R., Thermal radiation heat transfer, New York McGraw-Hill, 1972
[70] Ruan, L.M., Tan, H.P.,Yan, Y.Y., A monte carlo (MC) method applied to the medium with nongray absorbing-emitting-anisotropic scattering particles and gray approximation, Numerical Heat Transfer, Part A: Applications, 42(3), pp. 253-268, 2002
[71] Caliot, C., Eymet, V., El Hafi, M., Le Maoult, Y.,Flamant, G., Parametric study of radiative heat transfer in participating gas-solid flows, International Journal of Thermal Sciences, 47(11), pp. 1413-1421, 2008
[72] Buckius, R.O.,Tien, C.L., Infrared flame radiation, International Journal of Heat and Mass Transfer, 20(2), pp. 93-106, 1977
[73] Chang, H.,Charalampopoulos, T.T., Determination of the Wavelength Dependence of Refractive Indices of Flame Soot, Proceedings: Mathematical and Physical Sciences, 430(1880), pp. 577-591, 1990

[74] Goodwin, D.G.,Mitchner, M., Flyash radiative properties and effects on radiative heat transfer in coal-fired systems, International Journal of Heat and Mass Transfer, 32(4), pp. 627-638, 1989

[75] Mengüç, M.,Viskanta, R., Comparison of radiative transfer approximations for a highly forward scattering planar medium, Journal of Quantitative Spectroscopy and Radiative Transfer, 29(5), pp. 381-394, 1983

[76] Hunter, B.,Guo, Z., Phase-Function Normalization in the 3-D Discrete-Ordinates Solution of Radiative Transfer—PART I: Conservation of Scattered Energy and Asymmetry Factor, Numerical Heat Transfer, Part B: Fundamentals, 62(4), pp. 203-222, 2012

[77] Boulet, P., Collin, A.,Consalvi, J.L., On the finite volume method and the discrete ordinates method regarding radiative heat transfer in acute forward anisotropic scattering media, Journal of Quantitative Spectroscopy and Radiative Transfer, 104(3), pp. 460-473, 2007

[78] Bäckström, D., Johansson, R., Andersson, K., Johnsson, F., Clausen, S.,Fateev, A., Measurement and modeling of particle radiation in coal flames, Energy & Fuels, 28(3), pp. 2199-2210, 2014

[79] Solovjov, V.P., Lemonnier, D.,Webb, B.W., SLW-1 Modeling of Radiative Heat Transfer in Nonisothermal Nonhomogeneous Gas Mixtures with Soot, Journal of Heat Transfer, 133(10), pp. 9, 2011

[80] Felske, J.D.,Charalampopoulos, T.T., Gray gas weighting coefficients for arbitrary gas-soot mixtures, International Journal Heat Mass Transfer, 25(12), pp. 1849-1855, 1982

[81] A.Yu, S., Statistical modeling of thermal radiation transfer in buoyant turbulent diffusion flames, Combustion and Flame, 136(1-2), pp. 51-71, 2004

[82] Yin, C., Rosendahl, L.A.,Kær, S.K., Grate-firing of biomass for heat and power production, Progress in Energy and Combustion Science, 34(6), pp. 725-754, 2008

[83] Haukohl, J., Waste to energy state of the art report, 6th Edition, International Solid Waste Association Copenhagen, p. 210, 2012

[84] Bahador, M.,Sundén, B., Investigation on the effects of fly ash particles on the thermal radiation in biomass fired boilers, International Journal of Heat and Mass Transfer, 51(9-10), pp. 2411-2417, 2008

[85] Brunner, T., Fluch, J., Obernberger, I.,Warnecke, R., Investigations of aerosol formation pathways during MSW combustion based on high-temperature impactor measurements, Fuel Processing Technology, 105(0), pp. 154-160, 2013

[86] Wall, T.F., Lowe, A., Wibberley, L.J.,McC. Stewart, I., Mineral matter in coal and the thermal performance of large boilers, Progress in Energy and Combustion Science, 5(1), pp. 1-29, 1979

[87] Bhattacharya, S.P., A theoretical investigation of the influence of optical constants and particle size on the radiative properties and heat transfer involving ash clouds and deposits, Chemical Engineering and Processing: Process Intensification, 39(5), pp. 471-483, 2000

[88] Butler, B.,Webb, B., Local temperature and wall radiant heat flux measurements in an industrial scale coal fired boiler, Fuel, 70(12), pp. 1457-1464, 1991

[89] Lowe, A., Stewart, I.,Wall, T., The measurement and interpretation of radiation from fly ash particles in large pulverized coal flames, in Symposium (International) on Combustion. Elsevier,p. 105-114, 1979

[90] Andersson, K., Johansson, R., Hjärtstam, S., Johnsson, F.,Leckner, B., Radiation intensity of lignite-fired oxy-fuel flames, Experimental Thermal and Fluid Science, 33(1), pp. 67-76, 2008

[91] Andersson, K.,Johnsson, F., Flame and radiation characteristics of gas-fired O2/CO2 combustion, Fuel, 86(5–6), pp. 656-668, 2007

[92] Gebhardt, Z.,Tomeczek, J., The emissivity of natural gas diffusion flames, Gas Waerme International., 31(7/8), pp. 329-334, 1982

[93] Gunners, N.-E., Methods of measurement and measuring equipment for fire tests : joint inter-Scandinavian fire tests on lining materials for buildings at Copenhagen fire test house, Acta polytechnica Scandinavica. Civil engineering and building construction series. Ci, 0355-2705 Stockholm Ingeniörsvetenskapsakademin, p. 45, 1967

[94] Johansson, R., Modelling elements in conversion of solid fuels - fixed bed combustion and gaseous radiation, Ph. D. thesis, Institutionen för energi och miljö, Energiteknik: Chalmers University, p. 192, 2008

[95] Coelho, P.J., Numerical simulation of radiative heat transfer from non-gray gases in three-dimensional enclosures, Journal of Quantitative Spectroscopy and Radiative Transfer, 74(3), pp. 307-328, 2002

[96] Wen, C.Y.,Chaung, T.Z., Entrainment Coal Gasification Modeling, Industrial and Engineering Chemistry Process Design and Development, 18(4), pp. 684-695, 1979

[97] Smith, T.F., Shen, Z.F.,Friedman, J.N., Evaluation of Coefficients for the Weighted Sum of Gray Gases Model, ASME Journal of Heat Transfer, 104(4), pp. 602-608, 1982

[98] Johansson, R., Andersson, K., Leckner, B.,Thunman, H., Models for gaseous radiative heat transfer applied to oxy-fuel conditions in boilers, International Journal of Heat and Mass Transfer, 53(1-3), pp. 220-230, 2010